Lappeenranta
University of Technology

DEPARTMENT OF MATHEMATICS AND PHYSICS

MASTER'S THESIS

Galvanomagnetic effects in InGaAs nanostructure

Examiners: Professor, Ph.D. Erkki Lähderanta, Ph.D. Alexander Lashkul
Supervisors: Professor, Ph.D. Erkki Lähderanta, Ph.D.Alexander Lashkul

Lappeenranta, May 2013

Yulia Grebenyuk
yulia.grebenyuk28@gmail.com

ABSTRACT

Yulia Grebenyuk

Galvanomagnetic effects in InGaAs nanostructure

Faculty of Technology, Department of Mathematics and Physics, major subject Technical Physics

2013

Lappeenranta University of Technology

Thesis for the Degree of Master of Science in Technology

83 pages, 45 figures and 9 tables

Examiners: Professor, Ph.D. Erkki Lähderanta, Ph.D. Alexander Lashkul

Keywords: diluted magnetic semiconductors, two-dimensional structures, transverse magnetoresistance, longitudinal magnetoresistance, Hall effect, anomalous Hall effect, Shubnikov - de Haas oscillations, spin splitting, quantization of energy spectrum.

Investigation of galvanomagnetic effects in nanostructure GaAs/Mn/GaAs/$In_{0.15}Ga_{0.85}As$/ GaAs is presented. This nanostructure is classified as diluted magnetic semiconductor (DMS). Temperature dependence of transverse magnetoresistivity of the sample was studied. The anomalous Hall effect was detected and subtracted from the total Hall component. Special attention was paid to the measurements of Shubnikov-de Haas oscillations, which exists only in the case of magnetic field aligned perpendicularly to the plane of the sample. This confirms two-dimensional character of the hole energy spectrum in the quantum well. Such important characteristics as cyclotron mass, the Fermi energy and the Dingle temperature were calculated, using experimental data of Shubnikov-de Haas oscillations. The hole concentration and hole mobility in the quantum well also were estimated for the sample. At 4.2 K spin splitting of the maxima of transverse resistivity was observed and *g*-factor was calculated for that case. The values of the Dingle temperatures were obtained by two different approaches. From the comparison of these values it was concluded that the broadening of Landau levels in the investigated structure is mainly defined by the scattering of charge carriers on the defects of the crystal lattice.

ACKNOWLEDGMENTS

This Master's thesis was written in the Department of Mathematics and Physics at Lappeenranta University of Technology, Finland.

Firstly, I would like to thank Prof. Erkki Lahderanta for providing me an opportunity to study at Lappeenranta University of Technology and his constant help and support during the education process. Special gratitude I want to express to my supervisor Ph.D. Alexander V. Lashkul, whose scientific knowledge and permanently good mood allowed me to perform theoretical part of this work. I also wish to thank Mikhail A. Shakhov who guided and helped me to conduct the experiments and implement maintenance of the Pulsed Magnetic Field System.

Additionally, I would like to thank my friend Ksenia for all these days we spent together working on our diplomas in the university, for all coffee breaks and evenings in the gym.

Finally, the biggest thanks go to my mum and brother. Even 2000 km could not become an obstacle for their love and continual support of my spirit.

Yulia Grebenyuk

CONTENT

LIST OF SYMBOLS AND ACHRONYMS

SYMBOLS

A_T	amplitude of Shubnikov-de Haas oscillations
B	magnetic field induction
B_{max}	magnetic field induction in the position of maximum of Shubnikov-de Haas oscillations
B_{NS}	magnetic field induction in the position of maximum of Shubnikov-de Haas oscillations with taking into account spin splitting
B_{h}	magnetic field induction in the proximity of hysteresis loop
B_{0+}	magnetic field induction in the position of zero-plus maximum of Shubnikov-de Haas oscillations
$C_I, C_U, C_C, C_{I,C}$	coefficients for description of anisotropic magnetoresistance
c	speed of light
d	thickness of sample
E, E_x, E_y	electrical field intensity and its components
E_{F0}, E_F	Fermi energy
e	electron charge
H	magnetic field intensity
H_c	coercive force
g	g-factor
I	electric current
j	electric current density
k	wave vector
k_B	Boltzmann constant
L	integer
L_{ij}	distance between contacts of sample
M	magnetization
m	electron mass
m_c	cyclotron mass
m^*	effective mass
N_{Mn}	thickness of manganese layer

N_m	quantum number of Landau level
n	concentration of charge carriers
P	period of Shubnikov-de Haas oscillations
p_{SdH}	concentration of holes calculated from the parameters of Shubnikov-de Haas oscillations
p_{Hall}	concentration of holes calculated using the parameters of the Hall mobility
R_H	the Hall constant
R_{S}	the anomalous Hall coefficient
R_{xx}, R_{xy}	components of transverse resistance
$R_{\mathrm{xy}}{}^{\mathrm{n}}$, $R_{\mathrm{xy}}{}^{\mathrm{a}}$	normal and anomalous component of the Hall resistance, respectively
r	ratio between the spin and cyclotron splitting
S_m	cross-section of Fermi surface
T	temperature
T_{c}	Curie temperature
$T_{D,}T_{D_{Hall}}$, $T_{D_{ShH}}$	Dingle temperature, Dingle temperature calculated from the parameters of the Hall mobility and the parameters of Shubnikov-de Haas oscillations, respectively
T_{g}	structure growing temperature
U	the Hall voltage
W_{ij}	distance between contacts of sample
x, x_1, x_2	auxiliary parameters
β	auxiliary parameter for description of g-factor
γ	the Hall factor
$\Delta\varepsilon$	energy required for splitting of Landau level
Δ'	difference between values of reciprocal magnetic induction for non-splitted and splitted maxima
δ_1, δ_2	oscillating components of conductivity tensor
$\varepsilon, \varepsilon_0$	energy of electron
η	density of states
θ	angle between crystal direction and direction of current
θ'	angle between direction of magnetic field and normal to the plane of

	sample
μ	drift mobility
μ_H	the Hall mobility
μ_0	Bohr magneton
ξ_1, ξ_2	auxiliary parameters for description of components of conductivity tensor
ρ	resistivity
ρ_{av}	average of the longitudinal anisotropic magnetoresistivity over 360º in the plane of the sample
ρ_{xx}, ρ_{xy}	components of transverse resistivity
ρ_{xy}^{AH}	the anomalous Hall resistivity
ρ_{zz}	longitudinal resistivity
σ	conductivity
$\sigma_{cl}, \sigma_1, \sigma_2$	components of transverse conductivity
σ_{xx}, σ_{xy}	components of conductivity tensor
τ	mean free time
τ'	relaxation time
φ	angle between directions of magnetization and current
φ_H	the Hall angle
$\chi_\perp$	coefficient of transverse magnetoresistance
ψ	angle between crystal direction and direction of magnetization
Ω	auxiliary parameter for description of oscillating components of conductivity tensor
ω_c	cycloron frequency
$\hbar$	Planck constant

ACHRONYMS

ADC	analog-to-digital converter
AHE	the anomalous Hall effect
DAC	digital-to-analog converter
DMS	diluted magnetic semiconductors
PMFS	pulsed magnetic field system
QW	quantum well

1 INTRODUCTION

Due to their unique electrical and optical properties semiconductors play an important role in modern electronics [1]. Particularly, much attention has been attracted by diluted magnetic semiconductors (DMS), which combine the properties of both magnetic and semiconductor materials [2]. Semiconductors based on (Ga,Mn)As structures is the most intensively studied type of DMS [3] .

(Ga,Mn)As is III-V compound with typical concentrations of manganese equal to 3 - 10 % [4]. At low temperatures it exhibits ferromagnetic ordering [4]. The interaction of charge carriers (holes) with local spins causes the appearance of a range of interesting phenomena, as for example, the anomalous Hall effect [4]. The anomalous Hall effect is considered to be the main method of investigation of magnetization in two-dimensional DMS structures [5]. The latter is due to the fact that strong paramagnetic signal from the substrate interferes to detect the magnetic moment of ferromagnetic material when using traditional approach of measuring [5]. Although, it should be mentioned that most of previous studies of galvanomagnetic and transport properties of (Ga,Mn)As structures concerns three-dimensional samples. The necessity of further investigation of two-dimensional DMS structures is explained by their wide application in such devices as light-emitting diodes (LED) and metal-oxide-semiconductor MOS transistors [6].

Two-dimensional character of the hole energy spectrum in such materials is supported by the observation of Shubnikov–de Haas oscillations only in the case of magnetic field aligned perpendicularly to the plane of the sample [4, 6]. These oscillations represent oscillations of magnetoresistance with changing of the intensity of magnetic field [6]. In this work the studies of Shubnikov–de Haas oscillations as well as the phenomena of ordinary and anomalous Hall effects was conducted in diluted magnetic semiconductor with GaAs/Mn/GaAs/$In_{0.15}Ga_{0.85}As$/GaAs structure.

2 THEORETICAL BACKGROUND

2.1. Magnetoresistance

2.1.1. Conductivity tensor

Such important galvanomagnetic phenomena as magnetoresistance and the Hall effect can be described by electrical conductivity tensor. In [7] the components of this tensor are expressed as follows

$$\sigma_{xx} = \sigma_{yy} = \frac{e^2 n}{m}\xi_1, \tag{2.1}$$

$$\sigma_{xy} = -\sigma_{yx} = \omega_c \frac{e^2 n}{m}\xi_2, \tag{2.2}$$

$$\sigma_{zz} = \frac{e^2 n}{m}\tau' . \tag{2.3}$$

In these formulas e is an electron charge; n and m is concentration and mass of charge carriers, respectively, and τ' is relaxation time, which is an average of mean free time τ for all electrons. The formulas also include ξ_1 and ξ_2 which are defined in [7] in terms of τ and cyclotron frequency ω_c as

$$\xi_1 = < \frac{\tau}{1 + {\omega_c}^2 \tau^2} >, \tag{2.4}$$

$$\xi_2 = < \frac{\tau^2}{1 + {\omega_c}^2 \tau^2} > . \tag{2.5}$$

The cyclotron frequency ω_c is a frequency of uniform rotation of a particle in magnetic field [7]. The cyclotron frequency is not dependent on orbital radius or energy of this particle and defined as

$$\omega_c = \frac{eB}{m_c}, \tag{2.6}$$

where B is magnetic induction and m_c is cyclotron mass [7].

In the absence of magnetic field $\omega_c = 0$ and, therefore, $\sigma_{xy} = \sigma_{yx} = 0$ what means that in this case electrical conductivity becomes a scalar

$$\sigma = \frac{e^2 n}{m}\tau'. \tag{2.7}$$

2.1.2. Isotropic magnetoresistance

The change of resistance caused by magnetic field is called magnetoresistance [6]. Magnetoresistance is determined as $\Delta R/R(0)$, where $\Delta R(H) = R(H) - R(0)$; $R(H)$ is a resistance in applied magnetic field and $R(0)$ is resistance in zero field [8]. It is possible to distinguish transverse and longitudinal magnetoresistance depending on the direction of the current in the sample and applied magnetic field. When the magnetic field is perpendicular to the plane of the sample, one can observe the transverse magnetoresistance, otherwise, when the magnetic field is aligned parallel to the direction of current in the sample, the longitudinal magnetoresistance is observed.

In [7] it is shown that the transverse magnetoresistance is proportional to the square of magnetic induction

$$\frac{\Delta R}{R(0)} = \chi_\perp B^2, \tag{2.8}$$

where $\chi_\perp$ is a coefficient of transverse magnetoresistance. However, according to [7], this formula can be used only in the case of weak magnetic fields, which satisfy the condition

$$\omega_c \tau \ll 1. \tag{2.9}$$

In [9] the relation between transverse resistivity ρ of the sample in magnetic field and the components of electric conductivity tensor is deduced as

$$\rho(H) = \frac{\sigma_{xx}}{{\sigma_{xx}}^2 + {\sigma_{xy}}^2}. \tag{2.10}$$

It should be mentioned that this relation is correct for semiconductors with spherically symmetric isotropic energy band [9].

According to [9], for strong magnetic fields, for which the condition (2.9) is not satisfied, Eq. 2.8 can be simplified as

$$\rho(H) = \frac{\sigma_{xx}}{{\sigma_{xx}}^2 + {\sigma_{xy}}^2} \approx \frac{\sigma_{xx}}{{\sigma_{xy}}^2}. \tag{2.11}$$

The investigation of isotropic magnetoresistance for (Ga,Mn)As sample shows that the transverse resistance decreases with an increase of magnetic field [10]. It means that in this case negative magnetoresistance is observed. Fig. 2.1 demonstrates magnetic field dependencies of the resistivity of (Ga, Mn)As at different temperatures with magnetic field perpendicular to the plane. It should be also noticed that in Fig. 2.1 there is an interval of temperatures and the values of magnetic field induction where positive magnetoresistance is observed. It corresponds to the case of weak magnetic fields and temperatures, which are lower than the temperature of ferromagnetic transition T_c, called Curie temperature [10].

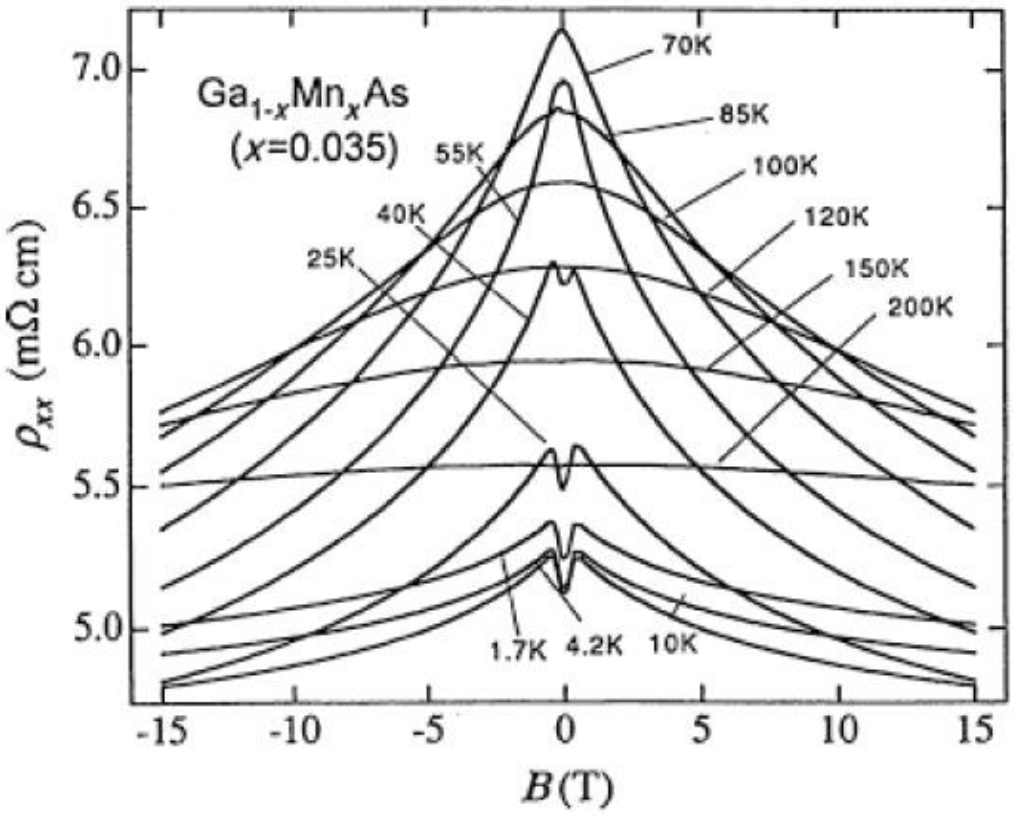

Figure 2.1. Magnetic field dependences of transverse resistivity of (Ga,Mn)As structure at different temperatures [10]. Above the temperature approximately 40 K only negative magnetoresistance is observed [10]. Below 40 K magnetoresistance is positive within short interval of magnetic field values [10].

2.1.3. Anisotropic magnetoresistance

In ferromagnetic semiconductor also magnetization influences on its resistance. That explains anisotropic magnetoresistance, which is defined by the difference between the longitudinal and transverse magnetoresistances [10]. Anisotropic magnetoresistance is a result of contribution of two components: non-crystalline component, which is due to the lower symmetry for different directions of the current, and crystalline component, which is explained by the crystal symmetry [10]. The longitudinal and transverse anisotropic magnetoresistance can be defined, respectively, by the following formulas

$$\frac{\Delta\rho_{xx}}{\rho_{av}} = C_I \cos(2\varphi) + C_U \cos(2\psi) + C_C \cos(4\psi) + C_{I,C} \cos(4\psi - 2\varphi), \quad (2.12)$$

$$\frac{\Delta\rho_{zz}}{\rho_{av}} = C_I \sin(2\varphi) - C_{I,C} \cos(4\psi - 2\varphi), \quad (2.13)$$

where $\Delta\rho_{xx} = \rho_{xx} - \rho_{av}$ and $\Delta\rho_{zz} = \rho_{zz} - \rho_{av}$; ρ_{av} is average of the longitudinal anisotropic magnetoresistivity over 360º in the plane of the sample; ψ is the angle between the crystal direction and its magnetization M; φ is the angle between the magnetization and the current I and C_I, C_U, C_C and $C_{I,C}$ are coefficients, which determine non-crystalline, the lowest order uniaxial, the lowest order cubic crystalline and crossed non-crystalline/crystalline terms, respectively [12,13].

Fig. 2.2a and 2.2b demonstrate for the sample of $Ga_{0.95}Mn_{0.05}As$ the longitudinal and transverse anisotropic magnetoresistance dependences on the angle between the magnetization and the current, the directions of which is mentioned in the legend. Fig. 2.2c illustrates the definition of the angles ψ and φ, as well as θ, which is the angle between the crystal direction and the current.

It should be noticed that graphs represented in Figs. 2.2a and 2.2b are shifted to zero along the ordinate axis, which was made in the purpose to emphasize the symmetries of the dependencies [10]. Moreover, it was stated that the main contribution to the anisotropic magnetoresistance of $Ga_{0.95}Mn_{0.05}As$ sample is made by non-crystalline component, while crystalline component is much weaker [12,13].

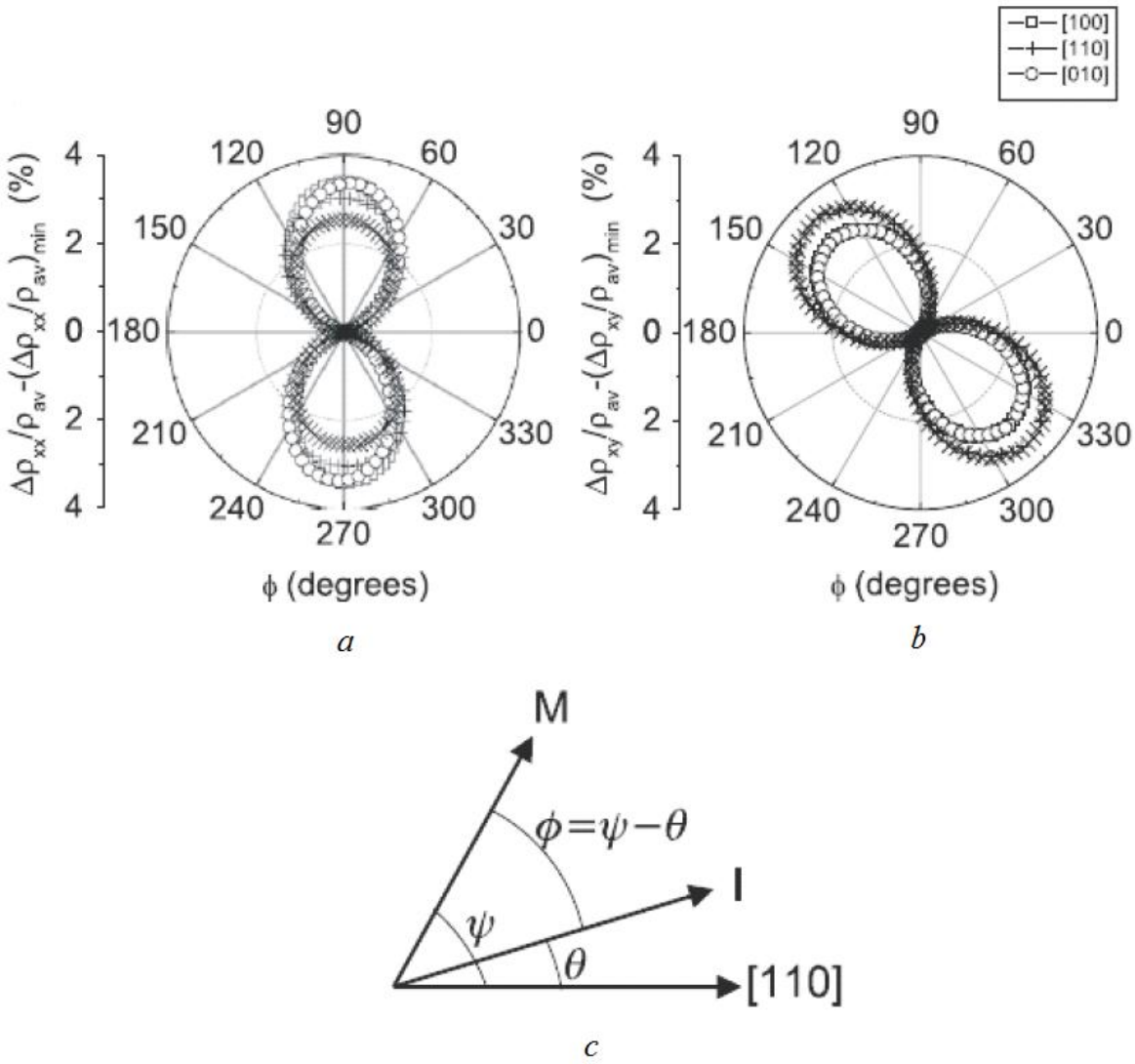

Figure 2.2. Angular dependence of the transverse (*a*) and longitudinal (*b*) anisotropic magnetoresistivity for the sample of $Ga_{0.95}Mn_{0.05}As$ [10]. Illustration of definition of the angles between the crystal direction, magnetization and the current (*c*) [10]. Here, φ is the angle between the magnetization *M* and the current *I*, ψ is the angle between the crystal direction and its magnetization and θ is the angle between the crystal direction and the current.

2.2. The Hall effect

2.2.1. Principal and main characteristics of the Hall effect

The Hall effect is a galvanomagnetic phenomenon, which occurs in a current-carrying conductor in transverse magnetic field. Under the influence of magnetic field, electromotive forces emerge inside the conductor and, therefore, additional electric field appears [7]. The main principle of this effect can be described by means of the following example.

A rectangular conductor with electrodes *a* and *b* on its lateral sides is shown in Fig. 2.3.

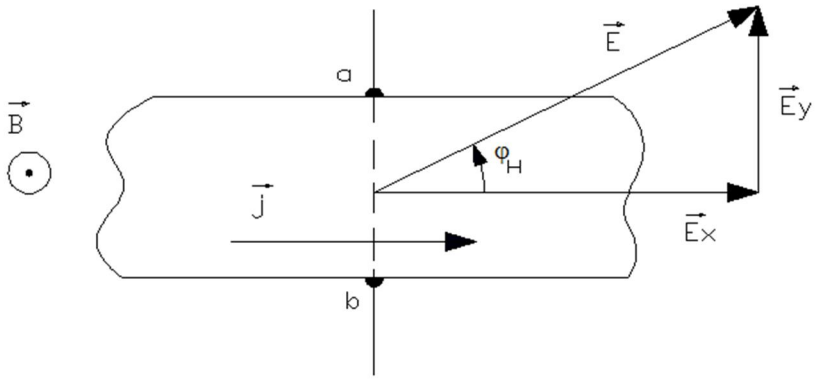

Figure 2.3. The Hall effect illustrated in a rectangular conductor [7].

The current density vector $\vec{j}$ and the magnetic induction vector $\vec{B}$ are aligned as it is displayed in Fig. 2.3. Taking into account an assumption of isotropy and homogeneity of the conductor, it is possible to declare that in the absence of magnetic field there is no potential difference between the electrodes *a* and *b* [7]. In this case, the electric field intensity $\vec{E}$ has the same direction as the current density vector $\vec{j}$ [7]. However, in the presence of magnetic field the potential difference between *a* and *b* appears and it changes its sign when the direction of current or magnetic field changes [7]. The appearance of the potential difference between *a* and *b* is due to the Lorentz force [7]. The Lorentz force is perpendicular to the direction of the current and magnetic field and pushes charge carriers to the lateral sides [14]. Thus, the resulting electric field consists of two components $\overrightarrow{E_x}$ and $\overrightarrow{E_y}$ and is turned by an angle φ_H

with respect to the current density vector $\vec{j}$ [7], as it is demonstrated in Fig. 2.3. This angle φ_H is called the Hall angle.

Connection between the electric field intensity E_y, the magnetic induction B, the Hall voltage U and the current inside of the conductor I can be expressed by the formula given in [7]

$$E_y = \frac{U}{d} = R_H B j = R_H B \frac{I}{ad}, \tag{2.14}$$

where d is a width of the sample, a is its size in the direction of magnetic field and R_H is a coefficient called the Hall constant.

The signs of the Hall constant and the Hall angle are defined by signs of charge carries, which participate in the process [7]. When the magnetic induction vector is directed as it is shown in Fig. 2.4*a* and charge carriers are holes, the Lorenz force is directed downwards with respect to the plane of the figure. It describes the case when the Hall constant and the Hall angle are considered to be positive. The opposite case with electrons as charge carriers is presented in Fig. 2.4*b*.

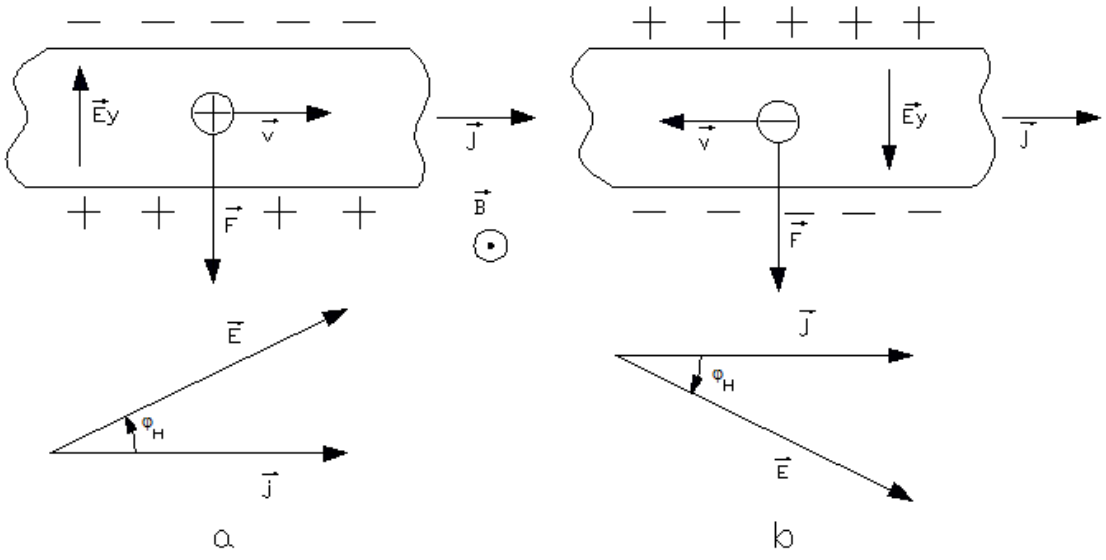

Figure 2.4. The determination of sign of the Hall angle: $\varphi_H > 0$ (*a*); $\varphi_H < 0$ (*b*) [7].

The Hall constant and the Hall angle can also be determined by the components of electrical conductivity tensor. According to [7], using Eqs. 2.1 and 2.2, it is possible to find the Hall angle as

$$tg\phi = \frac{\sigma_{xy}}{\sigma_{xx}} = \omega_c \frac{\xi_2}{\xi_1} = \frac{1}{c}\mu_H B\,, \tag{2.15}$$

where μ_H is the Hall mobility, which is described as

$$\mu_H = \frac{e}{m}\frac{\xi_2}{\xi_1}. \tag{2.16}$$

In [15] the connection between the Hall constant and the components of electric conductivity tensor for semiconductors with spherically symmetric isotropic energy band is presented in the following way

$$R_H = -\frac{1}{H}\frac{\sigma_{xy}}{{\sigma_{xx}}^2 + {\sigma_{xy}}^2}. \tag{2.17}$$

However, as it is shown in [15], for strong magnetic fields, which do not satisfy the condition (2.9) Eq. 2.17 can be simplified as

$$R_H = -\frac{1}{H}\frac{\sigma_{xy}}{{\sigma_{xx}}^2 + {\sigma_{xy}}^2} \approx -\frac{1}{H\sigma_{xy}}. \tag{2.18}$$

According to [7], for weak magnetic fields, when the condition (2.9) is not satisfied, the Hall constant is equal to the following expression

$$R_H \simeq \frac{\sigma_{xy}}{B\sigma^2} = \frac{tg\varphi_H}{B\sigma} = \gamma\frac{1}{cen} = \frac{1}{c\sigma}\mu_H\,. \tag{2.19}$$

Here c is speed of light and γ is the Hall factor, which is the ratio of drift and Hall mobilities [7]

$$\gamma = \frac{\mu_H}{\mu}. \tag{2.20}$$

Thereby, the basic principles and characteristics of the Hall effect have been described above. However, in ferromagnetic semiconductors this galvanomagnetic phenomenon has a special behavior, which is widely known as the anomalous Hall effect.

2.2.2. The anomalous Hall effect

Investigations of the Hall effect provide extraordinary results in ferromagnetic semiconductors. Such materials join ferromagnetic features and properties typical for semiconductors. Diluted magnetic semiconductor (DMS) is a common type of ferromagnetic semiconductors. Preparation of DMS includes the stage of doping a host material with a transition metal [16]. By means of such doping, d-electrons create local large magnetic moments and introduced carriers contributing to the formation of ferromagnetic binding between these moments [16].

According to [8], in ferromagnetic semiconductors the Hall resistivity includes two components: ordinary Hall component $R_{\mathrm{H}}(T)H$, which existence is explained by bias of electrons due to Lorentz force, and anomalous component $R_{\mathrm{S}}(T)M(T,H)$ as contribution from spontaneous magnetization

$$\rho_{\mathrm{xy}}(T,H) = R_{\mathrm{H}}(T)H + R_{\mathrm{S}}(T)M(T,H). \tag{2.21}$$

Here $R_{\mathrm{H}}(T)$ and $R_{\mathrm{S}}(T)$ are ordinary and anomalous Hall coefficient, respectively, and $M(T,H)$ is magnetization [8]. In comparison with the ordinary Hall coefficient, which mainly depends on the carrier concentration, the anomalous Hall coefficient depends on a wide range of parameters, for example, on the longitudinal resistivity ρ_{xx} [16].

In general, there are three main mechanisms, which may give rise to the anomalous Hall effect (AHE): intrinsic depletion, side jump and skew scattering [16]. In [17] it is shown that in the presence of external electric field applied to solids electrons receive an additional component to their group velocity. This component called Karplus-Luttinger's anomalous velocity mainly depends on the band structure and defines the intrinsic contribution to the AHE [16]. In [18] and [19] the theory about the major reason of origin of the AHE is proposed. This theory considers spin-orbit interaction in imperfect crystals as major reason of origin of the AHE. Such interaction cause skew scattering from impurities [16]. According to [20], side-jump of quasiparticles upon scattering from spin-orbit coupled impurities can be a source of the AHE. In real materials three mechanisms mentioned above contributes to emergence of the AHE [16]. The illustration of these mechanisms is presented in Fig. 2.5.

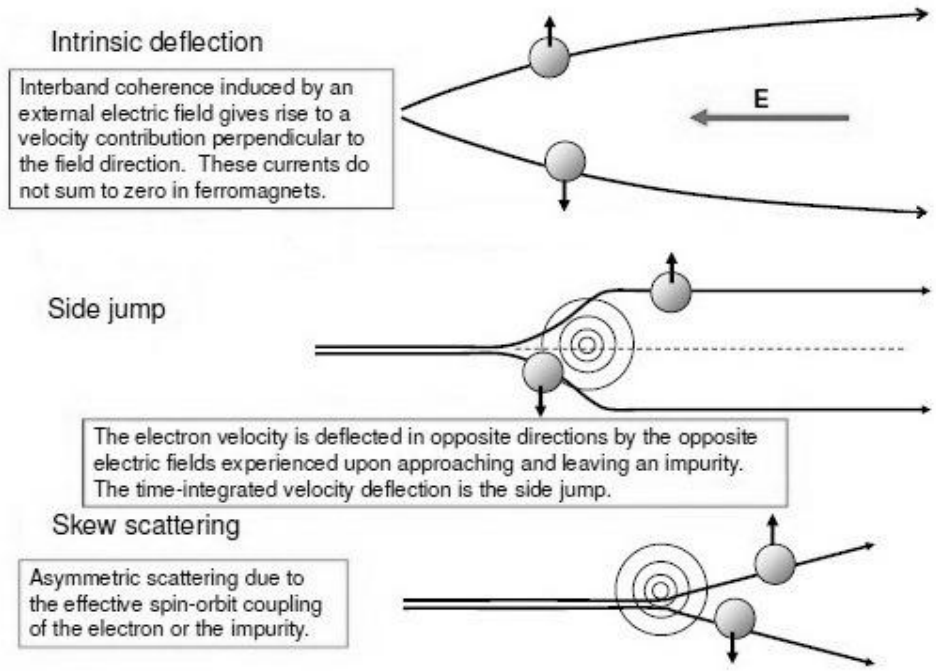

Figure 2.5. The main mechanisms of the occurrence of the anomalous Hall effect [9].

In [21], [22], [23] and [24] it is shown that the DMS systems based on (Ga,Mn)As structure have a scattering-independent mechanism in metallic regime and the anomalous component of the Hall effect is proportional to the square of the longitudinal resistivity

$$\rho_{xy}^{AH} \sim \rho_{xx}^{2}. \qquad (2.22)$$

In [21] the intrinsic mechanism is established as dominative in metallic regime of (Ga,Mn)As structures grown on InAs. The temperature dependencies of longitudinal ρ_{xx} and transverse ρ_{xy} resistivity of the investigated samples in the absence of magnetic field are shown in Fig. 2.6. The doping levels of manganese for certain samples are shown beside each curve. It should be noted that annealed samples (indicated in Fig. 2.6 as *) demonstrate weakly pronounced results for the transverse resistivity and have less values of the longitudinal resistivity as it can be seen from the comparison with the dependencies for the samples 0.05 and 0.05* [16]. The inset in Fig. 2.6 illustrates the magnetic field dependence of the transverse resistivity for the sample with content of manganese 7 % investigated at 10 K [16].

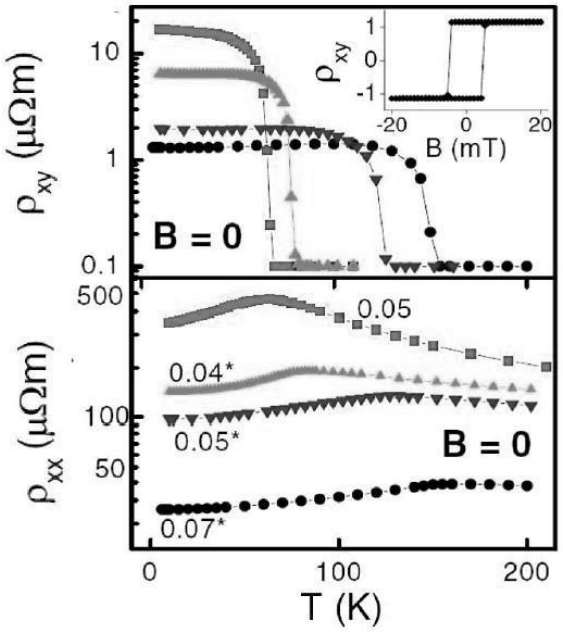

Figure 2.6. Temperature dependence of the transverse ρ_{xy} and longitudinal ρ_{xx} resistivity of (Ga,Mn)As structures grown on InAs in the absence of magnetic field [16]. Annealed samples (indicated as *) demonstrate weakly pronounced results for the transverse resistivity and have less values of the longitudinal resistivity [16]. Inset shows the magnetic field dependence of the transverse resistivity for the sample with content of manganese 7 % investigated at 10 K [16].

Experimentally the anomalous Hall component can be found in nonlinear character of the dependence of the total Hall resistivity on magnetic field under the condition that the latter is weak [11]. In comparison with it, in high magnetic fields when predominant contribution is made by the ordinary Hall component, the linear dependence is observed [11]. The nonlinearity of the total Hall resistivity is demonstrated in Fig. 2.7 and 2.8, which represents the dependence of the Hall resistivity on magnetic field for $Si_{1-x}Mn_x$/ Al_2O_3 and $Si_{1-x}Mn_x$/GaAs samples, respectively, at different temperatures. Table 2.1 contains the information about the parameters of these samples.

Table 2.1. Parameters of the investigated $Si_{1-x}Mn_x$ samples [11].

Sample number	Substrate	Thickness of the sample, *d*, nm	Coercive force, H_c, Oe at 80 K	AHE sign
1	Al_2O_3	57	2000	-
2	GaAs	80	0	+

It can be noticed from Figs. 2.7 and 2.8 that the Hall effect manifests itself stronger in the sample with GaAs substrate and has different signs for the samples: for $Si_{1-x}Mn_x$/ Al_2O_3 the Hall effect is negative and for $Si_{1-x}Mn_x$/GaAs it is positive. The important feature, which is demonstrated in Fig. 2.7, is the presence of the hysteresis loop being observed up to 230 K. The sample $Si_{1-x}Mn_x$/ Al_2O_3 demonstrates strong coercive force, which has a value of approximately 2 kOe at 100 K, while the anisotropy of the magnetic moment in the sample $Si_{1-x}Mn_x$/GaAs leads to the absence of the hysteresis loop in this sample [11].

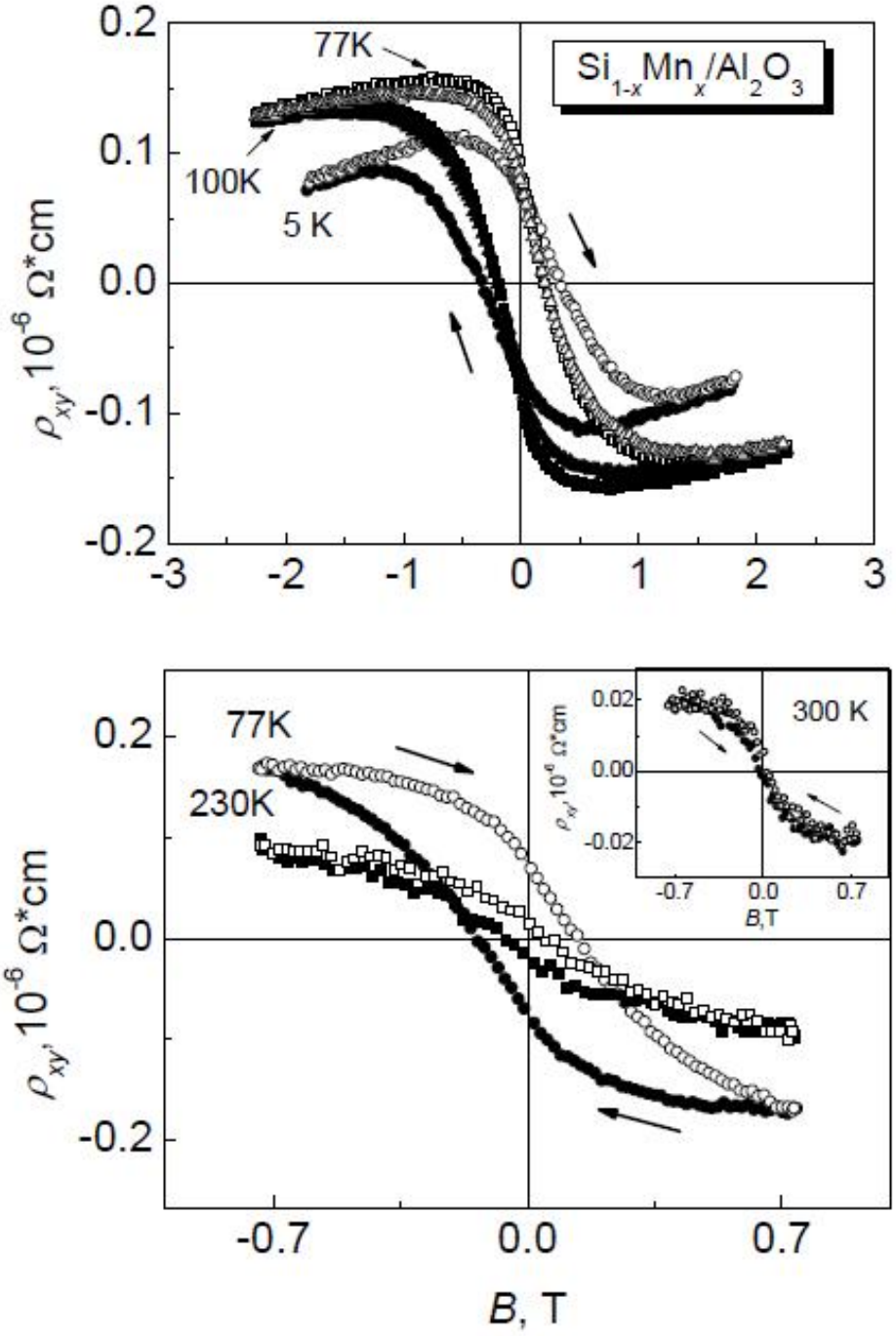

Figure 2.7. The dependencies of the Hall resistivity on magnetic field for $Si_{1-x}Mn_x$/ Al_2O_3 structure at different temperatures [11]. The main features of the dependences are the presence of the hysteresis loop, which is observed up to 230 K, and negative sign of the Hall effect [11]. Inset shows the dependence at room temperature [11].

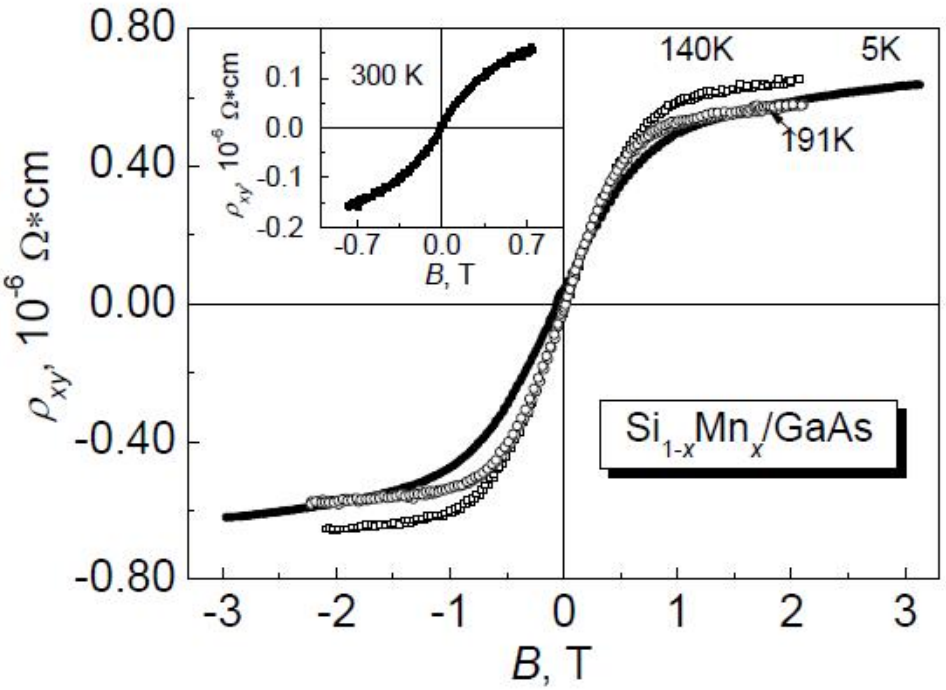

Figure 2.8. The dependencies of the Hall resistivity on magnetic field for $Si_{1-x}Mn_x$/ GaAs structure at different temperatures. The main features of the dependences are the absence of the hysteresis loop and positive sign of the Hall effect [11]. Inset shows the dependence at room temperature [11].

Currently, special attention is paid to the investigation of the Hall effect in semiconductors, which combine ferromagnetic and nonmagnetic material in their structure. For example, the spin-dependent scattering in semiconductors with trilayer structure (ferromagnet-nonmagnet-ferromagnet) was studied [25]. The results of measurement of the Hall resistivity in weak magnetic field for the structure (Ga,Mn)As/(Al,Ga)As/(Ga,Mn)As are demonstrated in Fig. 2.9. It can be clearly seen that there is a hysteresis loop near zero field for both values of temperatures. This is explained by the fact that magnetic easy-axis is directed perpendicularly to the plane of the sample [25]. Magnetic field dependence of the Hall resistivity was also investigated for (Ga,Mn)As in [25] and is illustrated in Fig. 2.10. Additionally, it was determined that there is a dependence of the ferromagnetic coupling between two layers on the thickness of the sample and the content of Al in nonmagnetic layer [25].

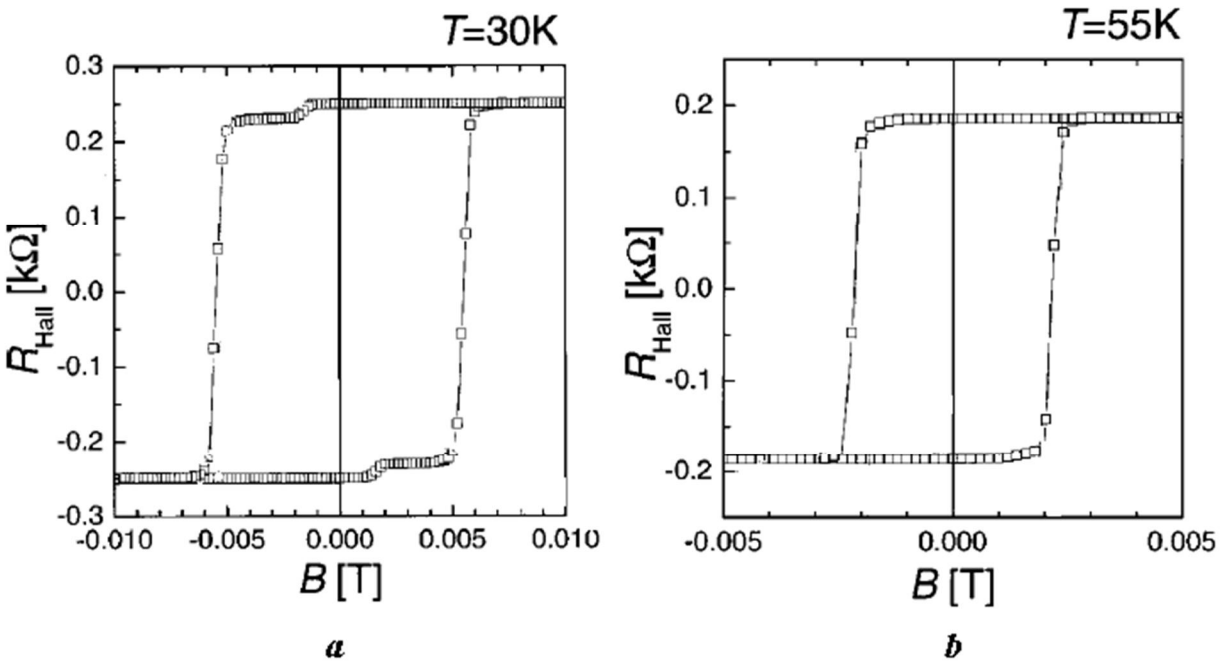

Figure 2.9. The hysteresis loop in magnetic field dependences of the Hall resistivity of Ga,Mn)As/(Al,Ga)As/(Ga,Mn)As structure at 30 K (*a*) and 55 K (*b*) [25].

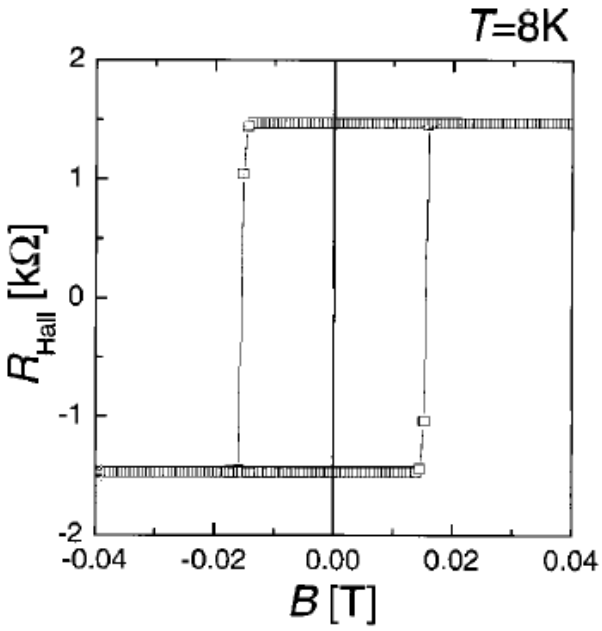

Figure 2.10. The hysteresis loop in magnetic field dependence of the Hall resistivity of (Ga,Mn)As structure at 8 K [25].

Thus, current investigation of the Hall effect experimentally proves the presence of the anomalous component of this phenomenon for ferromagnetic semiconductors, reveal the main mechanism of its appearance in these material and detect its peculiarities as, for example, the hysteresis loop in magnetic field dependence of the Hall resistivity. However, not all obtained results in this field have proper theoretical explanation, as well, as there is a distinction in the behavior of this galvanometric property for different materials. These aspects imply that there is a range of directions for future studies of the Hall effect.

2.3. Shubnikov-de Haas oscillations

2.3.1. Energy spectrum of electron in strong magnetic field

From the point of view of quantum mechanics there is a quantization of movement of electrons in strong magnetic field in the plane, which is perpendicular to the direction of magnetic field [26]. This causes the occurrence of allowed energy levels (Landau levels) with the distance between two neighboring ones equal to $\hbar\omega_c$, where $\hbar$ is the reduced Planck constant [9]. According to [9], the quantization of the energy spectrum can be neglected in high temperatures when

$$\hbar\omega_c \ll k_B T \,. \tag{2.23}$$

However, in case of strong magnetic fields and at low temperatures the condition (2.23) is not satisfied and such magnetic fields are called quantizing magnetic fields [9]. The dependence of energy ε on a wave vector k in the presence and the absence of quantizing magnetic field is shown in Fig. 2.11.

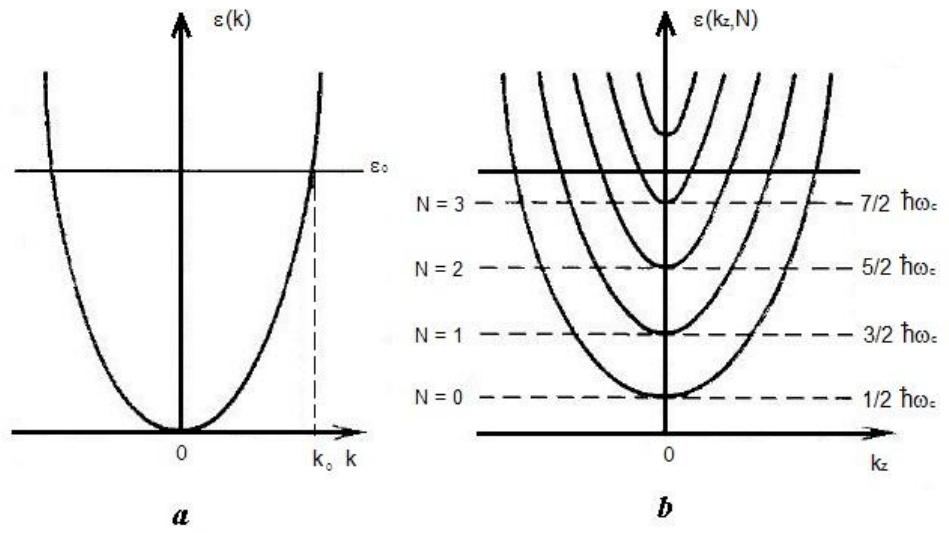

Figure 2.11. Dependences of energy on the wave vector in the absence (*a*) and presence (*b*) of magnetic field [9]. In the presence of strong magnetic field there is a quantization of the energy spectrum, which causes formation of Landau levels with the distance between two neighboring ones equal to $\hbar\omega_c$ [26].

The density of states $\eta(\varepsilon)$ of charge carriers in the presence of quantizing magnetic field can be described as it is presented in [27]

$$\eta(\varepsilon) = \frac{m^{\frac{3}{2}}}{\sqrt{2}\pi^2\hbar^3}\frac{\hbar\omega_c}{2}\sum_{N_m=0}^{N_{max}}\left[\varepsilon - (N_m + {}^1\!/_2)\hbar\omega_c\right]^{-\frac{1}{2}}. \quad (2.24)$$

Therefore, there are points $= (N_m + {}^1\!/_2)\hbar\omega_c$, in which $\eta(\varepsilon)$ tends to infinity. It means that the dependence $\eta(\varepsilon)$ has a discontinuous character that leads to the oscillation of transport properties [26]. The connection between this peculiarity and the Fermi energy can be expressed as

$$\frac{2}{3}\left(\frac{E_{F_0}}{\hbar\omega_c}\right) = \sum_{N_m=0}^{N_{max}}\left[\varepsilon - (N_m + {}^1\!/_2)\hbar\omega_c\right]^{\frac{1}{2}}, \quad (2.25)$$

$$E_{F_0} = \frac{\hbar^2}{2m}(3\pi^2 n)^{\frac{2}{3}}, \quad (2.26)$$

where E_{F_0} is the Fermi energy in the absence of magnetic field and n is concentration of charge carriers [26].

Thus, quantization of energy spectrum in magnetic field leads to the appearance of specific features in transport characteristics of semiconductor materials. One of these features is the oscillation of magnetoresistance, which is called Shubnikov-de Haas oscillations.

2.3.2. Calculation method for Shubnikov-de Haas oscillations

Shubnikov-de Haas oscillations are the oscillations of magnetoresistance with changing of the intensity of magnetic field [9]. They occur in a crystal under the condition of degenerate electron gas [9]. Shubnikov-de Haas oscillations are due to the fact that change of the magnitude of magnetic field causes periodical change of density of states on the Fermi level [26].

According to [26], in order to observe Shubnikov-de Haas oscillations the simultaneous satisfaction of the following three conditions is obligatory

$$\omega_c \tau \gg 1, \tag{2.27}$$

$$\hbar\omega_c > k_B T, \tag{2.28}$$

$$E_{F0} > \hbar\omega_c . \tag{2.29}$$

The condition (2.27) is a consequence of the uncertainty principle and means that the distance between two neighboring Landau levels $\hbar\omega_c$ should exceed the broadening of each level $\hbar/\tau$ [26]. The condition (2.28) implies that the thermal broadening should be less than the distance between two neighboring Landau levels $\hbar\omega_c$[26]. The condition (2.29) limits the magnitude of magnetic field for observation of Shubnikov-de Haas oscillations [26]. The combination of

the conditions (2.27) and (2.28) defines that the oscillations occur in degenerate electron gas [26].

In [27] the formula for calculation of the transverse conductivity σ_{xx} was deduced as

$$\sigma_{xx} = \sigma_{cl} + \sigma_1 + \sigma_2 , \tag{2.30}$$

where σ_{cl} represents the conductivity in the case of large quantum numbers and is approximately equal to

$$\sigma_{cl} = \frac{e^2 n}{m\tau {\omega_c}^2}. \tag{2.31}$$

The explicit expressions for two other components $\sigma_1$and σ_2 is written in [27] as

$$\frac{\sigma_1}{\sigma_{cl}} = \frac{5x}{\sqrt{2}}\left(\frac{\hbar\omega_c}{E_F}\right)^{\frac{1}{2}} \sum_{M=1}^{\infty} \frac{(-1)^M M^{\frac{1}{2}}}{sh(Mx)} \exp\left(-\frac{2\pi M}{\omega_c \tau'}\right) \cos\left(\frac{2\pi M E_F}{\hbar\omega_c} - \frac{\pi}{4}\right), \tag{2.32}$$

$$\frac{\sigma_2}{\sigma_{cl}} = \frac{3\pi x}{8}\left(\frac{\hbar\omega_c}{E_F}\right) \sum_{M=1}^{\infty} \frac{(-1)^M M^{\frac{1}{2}}}{sh(Mx)} \exp\left(-\frac{2\pi M}{\omega_c \tau'}\right) \cos\left(\frac{2\pi M E_F}{\hbar\omega_c} - \frac{\pi}{2}\right). \tag{2.33}$$

These components have dominate character in the case of small and large amplitudes of oscillations, respectively [26].

According to [26], the period of Shubnikov-de Haas oscillations is connected to the extremal cross-section of Fermi surface S_m by the plane perpendicular to $\vec{B}$

$$P = \frac{2\pi e}{\hbar S_m}. \tag{2.34}$$

Defects of the crystal structure and inhomogeneity of the investigated samples cause non-thermal broadening of Landau levels [26]. The Dingle temperature T_D is the value, which takes this into account and is determined as

$$T_D = \frac{\hbar e}{\pi k_B m_c \mu_{\mathrm{H}}}, \tag{2.35}$$

where m_c is the cyclotron mass and μ_{H} is the Hall mobility [26].

The calculation of the cyclotron mass is carried out under the assumption of independence of the Dingle temperature vs. temperature [27]. In [26] the transcendental equation connects the values of amplitudes of Shubnikov-de Haas oscillations A for two definite temperatures and positions of maxima in magnetic field

$$\frac{A_1}{A_2} = \frac{x_1/sh(x_1)}{x_2/sh(x_2)}. \tag{2.36}$$

According to [26], x_1 and x_2 in this formula are introduced as

$$x_1 = \frac{2\pi^2 k_B}{\hbar e}\frac{m_c}{m_0}\frac{T_1}{B_1}, \tag{2.37}$$

$$x_2 = \frac{2\pi^2 k_B}{\hbar e}\frac{m_c}{m_0}\frac{T_2}{B_2}. \tag{2.38}$$

By means of numerical or graphical methods it is possible to solve Eq. 2.47 and estimate the value of the cyclotron mass.

In order to determine the position of maxima of Shubnikov-de Haas oscillations B_{max} it is necessary to take into consideration the dependence of the Fermi energy on magnetic field [26]. In [26] the following formula is suggested for the case of isotropic quadratic dispersion law

$$\frac{1}{B_{max}} = P_{is}\left[\left(L+\frac{1}{2}\right)^{\frac{3}{2}} - \left(\frac{1}{2}\right)^{\frac{3}{2}}\right]^{\frac{2}{3}}, \tag{2.39}$$

where L is integer. The analysis of this formula shows that the dependence of the Fermi energy on magnetic field is important for taking into account only in the case of calculation of positions of the first three maxima $N_L < 3$, otherwise, it can be neglected [26].

2.3.3. Spin splitting of Landau levels

In [9] energy of electron in magnetic field with taking into account the spin is defined as

$$\varepsilon(N_m, k_z, \sigma) = \left(N_m + \frac{1}{2}\right)\hbar\omega_c + {\hbar^2 k_z^2}/{2m^*} + \sigma g \mu_0 H. \tag{2.40}$$

According to [9], in this formula m^* is an effective mass, H is an intensity of magnetic field, σ is a spin projections equal to $\pm {1}/{2}$, g is a factor of spin splitting of energy of electron and μ_0 is Bohr magneton, which is determined as

$$\mu_0 = \frac{e\hbar}{2mc}. \tag{2.41}$$

The splitting of every Landau level leads to appearance of two sublevels [9]. Energy $\Delta\varepsilon$ required for it can be estimated by the following expression provided in [9]

$$\Delta\varepsilon = \varepsilon\left(N_m, \frac{1}{2}\right) - \varepsilon\left(N_m, -\frac{1}{2}\right) = \sigma g \mu_0 H. \tag{2.42}$$

Thus, besides the cyclotron quantization the appearance of spin sublevels takes place in magnetic field [28]. Spin splitting is not usually observed in bulk material, for which

$\Delta\varepsilon \ll \hbar\omega_c$, and appears only in strong magnetic fields where the amplitude of oscillations is significantly larger [28]. However, for two-dimensional systems $\Delta\varepsilon$ and $\hbar\omega_c$ have comparable values and the changes in behavior of the oscillations are noticeable [28].

In [28] the conductivity tensor for two-dimensional system is derived under the condition of small-amplitude of Shubnikov-de Haas oscillations

$$\sigma_{xx} = \frac{ne^2\tau/m}{1+\Omega^2}\left\{1 + \frac{2\Omega^2}{1+\Omega^2}\delta_1 + \left[\frac{2\Omega^2}{1+\Omega^2}\left(1-\frac{2\pi}{\Omega}\right) - \frac{(3-\Omega^2)\Omega^2}{(1+\Omega^2)^2}\right]\delta_2\right\}, \quad (2.43)$$

$$\sigma_{xy} = \frac{ne^2\tau/m}{1+\Omega^2}\left\{1 - \frac{1+3\Omega^2}{(1+\Omega^2)^2}\delta_1 + \left[\frac{1+3\Omega^2}{(1+\Omega^2)^2}\left(1-\frac{2\pi}{\Omega}\right) - \frac{1-3\Omega^2}{(1+\Omega^2)^2}\right]\delta_2\right\}. \quad (2.44)$$

In Eqs. 2.43 and 2.44 δ_1 and δ_2 are the oscillating components of the first and second order of smallness, correspondingly,

$$\delta_1 = 2\exp\left(-\frac{\pi}{\omega_c\tau}\right)\cos\left(2\pi\frac{E_F}{\hbar\omega_c} - \pi\right)\cos\left(\pi\frac{\Delta\varepsilon}{\hbar\omega_c}\right), \quad (2.45)$$

$$\delta_2 = 2\exp\left(-\frac{2\pi}{\omega_c\tau}\right)\cos\left(4\pi\frac{E_F}{\hbar\omega_c}\right)\cos\left(2\pi\frac{\Delta\varepsilon}{\hbar\omega_c}\right), \quad (2.46)$$

n is the total electron concentration and $\Omega = \omega_c\tau$ [28].

Fig. 2.12 demonstrates theoretical $\rho_{xx}(B)/\rho_{xx}(0)$ dependences on magnetic field for different ratio between the spin and cyclotron splitting $r = {\Delta\varepsilon}/{\hbar\omega_c}$. It is possible to change the ratio r by directing $\vec{B}$ with respect to the plane of the investigated sample due to the fact that cyclotron splitting depends primarily on perpendicular component of magnetic field, while spin splitting depends on the total magnetic field. It is illustrated in Fig. 2.12 that in the absence of spin splitting ($r = 0$) Shubnikov-de Haas oscillations are characterized by harmonic $\cos(\frac{2\pi E_F}{\hbar\omega_c})$ [28]. When $\Delta\varepsilon$ and $\hbar\omega_c$ become comparable, additional factors $\cos(\frac{\pi\Delta\varepsilon}{\hbar\omega_c})$

and $\cos(2\pi\Delta\varepsilon/\hbar\omega_c)$ appear, which correspond to δ_1 and δ_2, respectively [28]. In the case of half-integer r = 1/2, 3/2,… the oscillations are determined by the component δ_2 that leads to the doubling of oscillation frequency and the reduction of amplitude, meanwhile in the case of integer r the oscillations are determined again by harmonic $\cos(2\pi\Delta\varepsilon/\hbar\omega_c)$ [28]. However, it should be noticed that positions of maxima and minima alternate depending on integer r.

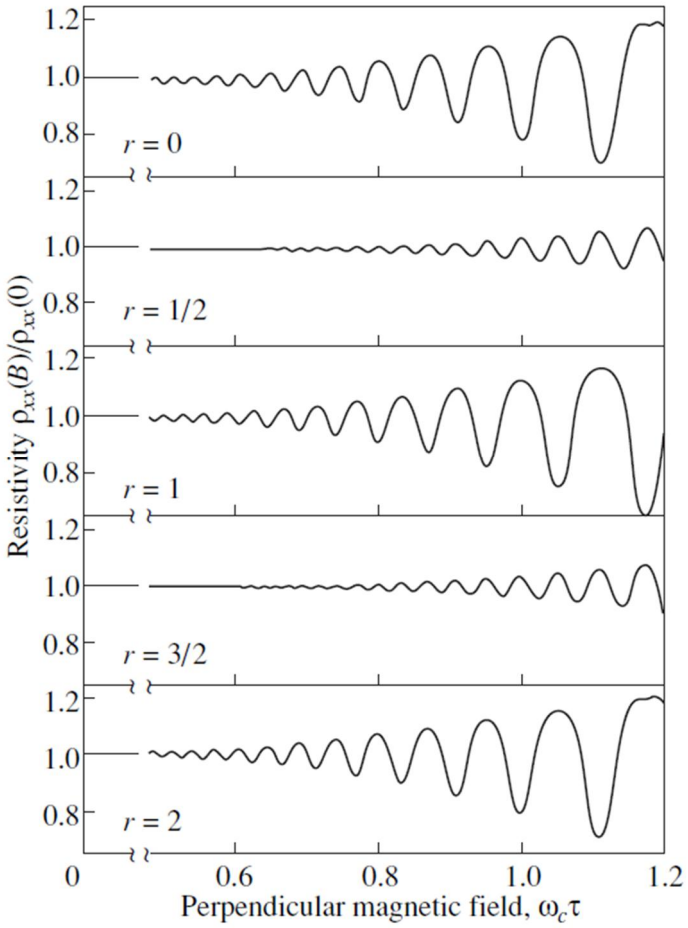

Figure 2.12. Theoretical dependences of $\rho_{xx}(B)/\rho_{xx}(0)$ on magnetic field for different ratio between the spin and cyclotron splitting r [28]. In the absence of spin splitting (r = 0) Shubnikov-de Haas oscillations are characterized by harmonic $\cos(2\pi E_F/\hbar\omega_c)$. In the case of half-integer r = 1/2, 3/2,… oscillation frequency are doubled and amplitude of oscillations decreases [28]. In the case of integer r the oscillations are determined again by harmonic $\cos(2\pi\Delta\varepsilon/\hbar\omega_c)$ [28]. Positions of maxima and minima alternate depending on integer r [28].

In [26] the formula for calculation of the position of maximum of Shubnikov-de Haas oscillations B_{NS} with taking the spin splitting of Landau levels into account is presented as

$$B_{NS} = (2\pi^4)^{\frac{1}{3}} \frac{\hbar}{e} n^{\frac{2}{3}} \left[\sum_{L=0}^{N_L} \left[L^{\frac{1}{2}} + (L + s\beta)^{\frac{1}{2}} \right] + 0.53 \left(\frac{k_B T}{\hbar \omega_c} \right)^{\frac{1}{2}} \right]^{-\frac{2}{3}}. \quad (2.47)$$

According to [26], component $0.53 \left(\frac{k_B T}{\hbar \omega_c} \right)^{\frac{1}{2}}$ in this formula is the temperature correction for the case of $T > T_D$; $s = \pm 1$ and β is introduced through the g-factor of spin splitting as

$$\beta = \frac{g m_c}{2m}. \quad (2.48)$$

The determination of g-factor is possible from the following expression for calculation of zero–plus maximum B_{0+} , provided in [27]

$$B_{0+} = \frac{\hbar}{e} \left[\frac{4\pi^2 n^2}{|g|} \frac{m}{m_c} \right]^{\frac{1}{3}}. \quad (2.49)$$

It should be also noticed that the existence of zero-minus maximum is impossible as it is clearly seen from Eq. 2.47 [26].

2.3.4. Temperature and angular dependences of Shubnikov-de Haas oscillations

The investigations of Shubnikov-de Haas oscillations were carried out in $GdTiO_3/SrTiO_3$ heterojunction [29]. In Fig. 2.13 the dependencies of the oscillating component of the resistance on the reciprocal magnetic field induction for $GdTiO_3/SrTiO_3$ structure are presented at different temperatures. As it can be clearly seen from Fig. 2.13, the amplitudes of oscillations raises with decrease of temperature, moreover, this peculiarity is better observed in strong magnetic fields [29].

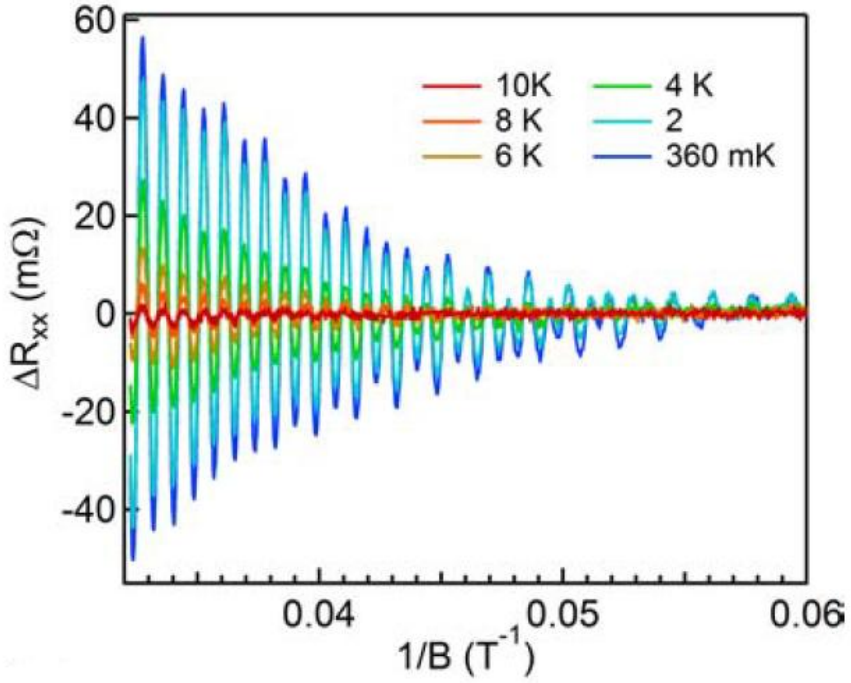

Figure 2.13. The dependencies of the oscillating component of the resistance on the reciprocal magnetic field induction for $GdTiO_3/SrTiO_3$ structure at different temperatures [29].

It should be also mentioned that in order to obtain the dependence presented in Fig. 2.16 the non-oscillating background was deducted from the full signal by means of using multiple polynomial fits [29].

The oscillations of Shubnikov-de Haas are also influenced by the angle θ' between the direction of magnetic field and normal to the plane of the sample [29]. Fig. 2.14 demonstrates the dependences of the oscillating component of the resistance on magnetic field for heterojunction $GdTiO_3/SrTiO_3$ at different angles from 0º, which is correspond to the case when magnetic field is perpendicular to the plane of the sample, to 50º. The main features of these dependencies are that the positions of maxima and minima of the oscillating component corresponds to approximately the same values of $1/Bcos(\theta')$ for all curves [29].

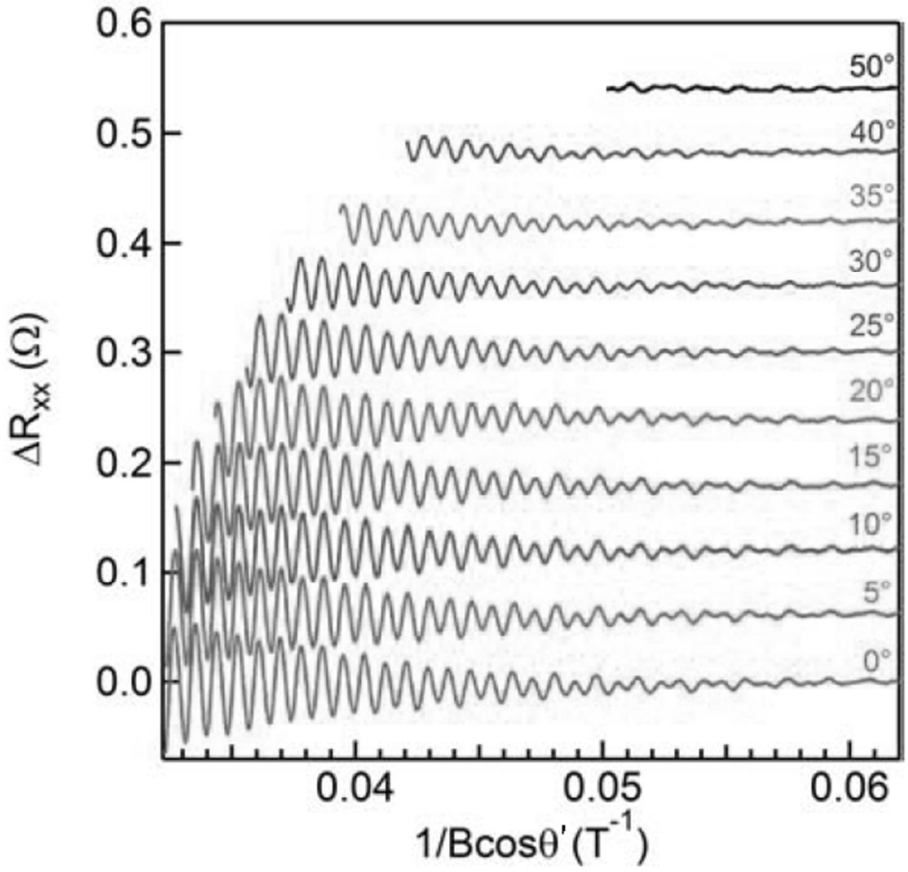

Figure 2.14. The dependences of the oscillating component of the resistance on the reciprocal of magnetic field induction for $GdTiO_3/SrTiO_3$ structure at different θ' [29].

As it was described above, the investigation of Shubnikov-de Haas oscillations can provide information about such important characteristics of energy spectrum theory as cyclotron mass, the Dingle temperature and *g*-factor as well as develop theoretical models for description of spin splitting. Moreover, the study of Shubnikov-de Haas oscillations allows revealing and confirming two-dimensional character of energy spectrum of charge carriers in quantizing magnetic field.

3 MAIN PROPERTIES OF InGaAs AND STRUCTURES BASED ON InGaAs

The investigated sample is classified as ferromagnetic semiconductor structure, particularly, diluted magnetic semiconductor. High Curie temperature T_c is one of the main characteristics of such materials [6]. This provides an opportunity to use them as a basic material in spintronic devices [6]. In this work special attention is paid to study of two-dimensional character of the hole energy spectrum and the possibility of observation of Shubnikov–de Haas oscillations is an important feature of the investigated material. This feature appeared because of high hole mobility of material due to the specific method of preparation of the sample [6]. The absence of Shubnikov–de Haas oscillations when magnetic field is applied in longitudinal direction with respect to the plane of the sample supports the prediction of two-dimensional character of the hole energy spectrum [6]. Moreover, in the investigated material it is possible to observe such transport phenomena as magnetoresistance, the Hall effect and the anomalous Hall effect. It should be also mentioned that currently the measurements of the anomalous Hall effect is the main way to investigate magnetization in two-dimensional DMS structures [5].

3.1. Structure

The structure of investigated material is GaAs/Mn/GaAs/$In_{0.15}Ga_{0.85}As$/GaAs sandwich [5]. It comprises $In_{0.15}Ga_{0.85}As$ quantum well (QW) with approximately 10 nm thickness [5]. The sample structure is presented in Fig. 3.1. The quantum well with spacers and buffer layer were grown by MOS – hydride epitaxy at 600 ºC and GaAs cap layer at 450 ºC [6]. By means of laser ablation, δ-layer of Mn atoms at concentration of 2 x 10^{14} cm^{-2} was deposited. Furthermore, for the compensation of the effect of depletion of the QW, δ-layer of C atoms (2 x 10^{14} cm^{-2}) was added to the structure [7].

In order to obtain high charge carrier mobility it is necessary to prevent the penetration of Mn atoms inside the quantum well. For that reason additional layer of GaAs is located between the QW and δ-layer of Mn atoms. The optimal thickness of this spacer layer is 3 nm, which provides strong enough interaction between carriers and Mn and at the same time do not allow Mn atoms penetrate into the QW [5].

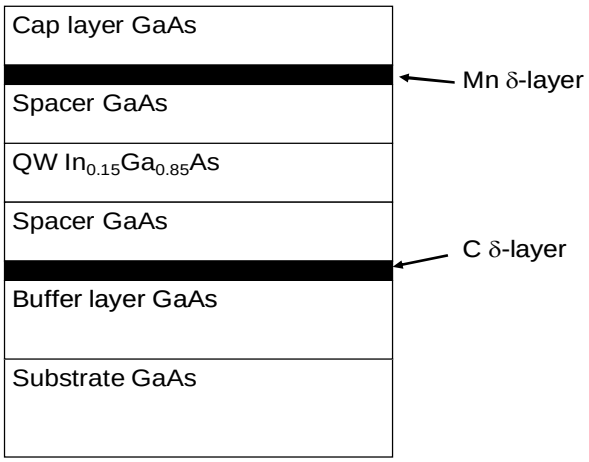

Figure 3.1. GaAs/Mn/GaAs/$In_{0.15}Ga_{0.85}As$/GaAs sandwich with δ-layers of manganese (2 x 10^{14} cm^{-2}) and carbon (2 x 10^{14} cm^{-2}) and $In_xGa_{1-x}As$ quantum well (10 nm) [6].

3.2. Review of earlier results

In [6] are presented earlier results of investigation of GaAs/Mn/GaAs/$In_xGa_{1-x}As$/GaAs structure. The parameters of the investigated samples can be seen in Table 3.1. The sample No. 4 is doped by carbon instead of manganese.

In these structures temperature dependences of electrical resistance $R_{xx}(T)$ were investigated (see Fig. 3.2). As it can be seen, the decrease of temperature leads to noticeable increase of electrical resistance of the sample No.1 and almost has no influence on this characteristic for the samples Nos. 2 and 3. It shows that the sample No.1 has conductivity of activation nature and the samples Nos. 2 and 3 present quasi-metallic behavior [6].

Table 3.1. Parameters of the investigated samples [6].

Sample	x	Thickness of Mn layer, N_{Mn} , ML
No. 1	0.16	1.20
No. 2	0.21	0.51
No. 3	0.23	0.40
No. 4	0.18	0

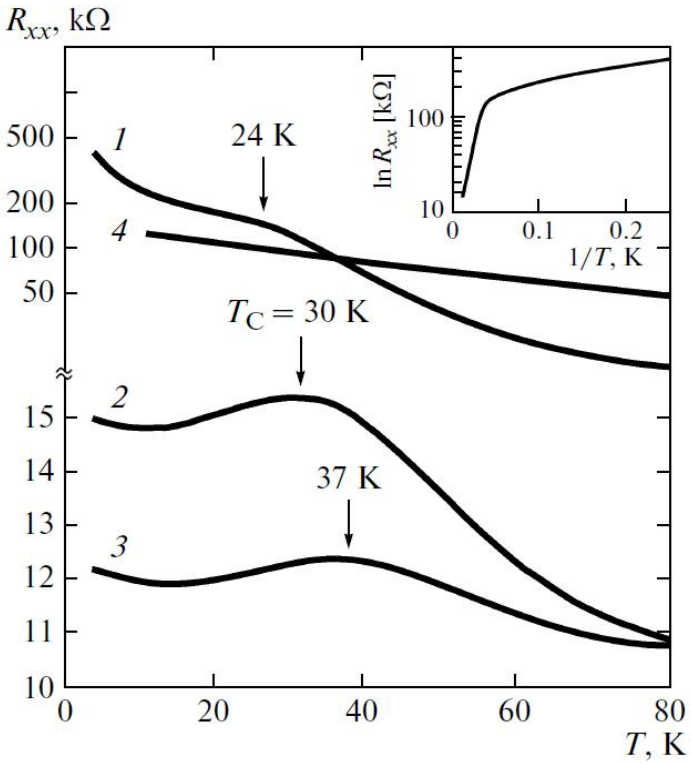

Figure 3.2. Temperature dependences of electrical resistance for different GaAs/Mn/GaAs/$In_xGa_{1-x}As$/GaAs structures [6]. This shows the activation nature of conductivity for the sample No. 1 and quasi-metallic behavior for the samples Nos. 2 and 3 [6]. The arrows indicate the Curie temperatures T_c of each sample [6].

Moreover, the dependences presented in Fig. 3.2 demonstrate the existence of characteristic points: the point of inflection for sample No.1 (see the inset to Fig. 3.2) and the maxima for Nos. 2 and 3, which are indicated by arrows. It also should be noted that for the sample No. 4

there is no such points and the electrical resistance for this sample is approximately proportional to temperature. The characteristic points are due to ferromagnetic properties of the investigated material and reflect Curie temperatures T_c when the material undergoes ferromagnetic transition [6].

The Shubnikov–de Haas oscillations are well-pronounced for the sample No. 2 and are shown in Fig. 3.3. They demonstrate the behavior of the transverse resistance R_{xx} when magnetic field is directed perpendicularly with respect to the plane of the sample. The inset of Fig. 3.3 illustrates the dependence of ratio of the transverse resistance R_{xx} to the transverse resistance in zero field $R_{xx}(0)$ on the magnetic field when it is parallel to the plane of the sample. This dependence shows the absence of Shubnikov–de Haas oscillations. Thus, the presence of Shubnikov–de Haas oscillations only in case of perpendicularly aligned magnetic field confirms the two-dimensional configuration [6].

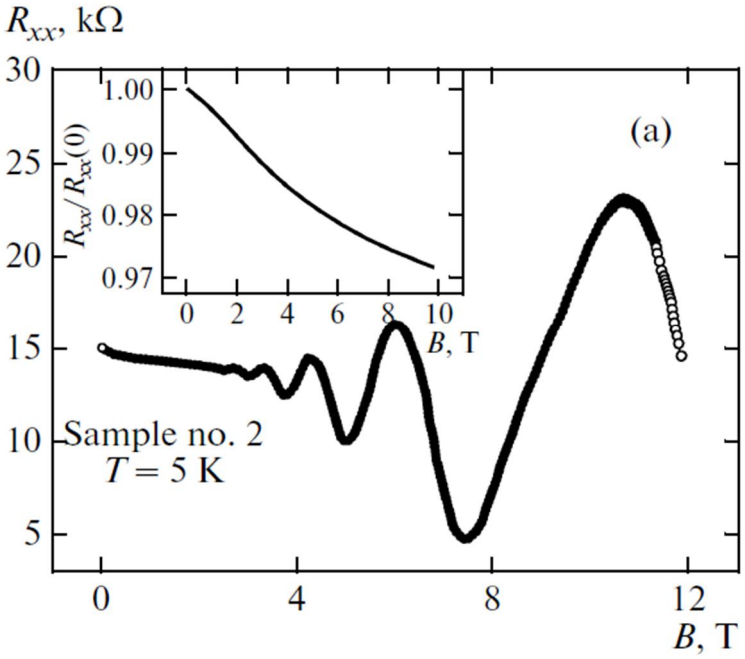

Figure 3.3. Magnetic field dependences of the transverse resistance for structure GaAs/Mn/GaAs/$In_xGa_{1-x}As$/GaAs [6]. Inset shows the dependence of ratio of the transverse resistance R_{xx} to the transverse resistance in zero field $R_{xx}(0)$ on the magnetic field when it is parallel to the plane of the sample [6].

The anomalous Hall effect for the samples Nos. 1 and 2 is detected in weak magnetic fields and its illustration for these samples is presented in Fig. 3.4. The upper insets of Fig. 3.4 demonstrate magnetic field dependences of the total Hall resistance for these samples. In order to obtain the anomalous component R_{xy}^{a} of the Hall resistance R_{xy}, the normal component R_{xy}^{n} was separated by special technique [6]. First, the constant R_H of the normal component R_{xy}^{n} was measured in strong magnetic fields when $R_{xy}^{n} >> R_{xy}^{a}$ [6]. Then the corresponding magnitude of it in weak magnetic fields was determined and subtracted from the total Hall resistance (see Eq.2.22) [6]. The occurrence of the anomalous Hall effect in the sample implies the spin polarization of holes in the channel, which indicates their interaction with manganese atoms and the establishment of ferromagnetic ordering [6].

The results of the investigation of GaAs/Mn/GaAs/$In_xGa_{1-x}As$/GaAs structure are also presented in [5]. The parameters of the samples under investigation were measured using X-ray diffraction technique and are shown in Table 3.2 [5].

Table 3.2. Parameters of the investigated samples [5].

Sample	x	Thickness of Mn layer, N_{Mn} , ML
A	0.21	0.5
B	0.16	1.8
C	0.18	0

In Fig. 3.5 temperature dependences of the resistance of GaAs/Mn/GaAs/$In_xGa_{1-x}As$/GaAs samples are presented. In this figure curves B and C corresponds to the left ordinate axis, which is logarithmic, while curve A corresponds to the right linear axis. This was done in the purpose to arrange obtained curves in one figure despite of the fact that temperature dependence of the resistance for the samples B is much stronger than for the sample A. It is clearly seen that the character of obtained curves is similar to the character of the curves presented in Fig. 3.2. For the sample with zero content of manganese (C) there is no maximum or point of inflection (the Curie point). However, for A and B they are observed. This is typical for magnetically ordered DMS. Such behavior of the resistance of the samples A and B can be explained by the assumption of spin-dependent nature of scattering and the

decrease of its rate [5]. When the direction of spins of the carriers coincides with the direction of magnetic moments, it leads to the increase of the mobility of carriers and, correspondingly, to the growth of the conductivity [5].

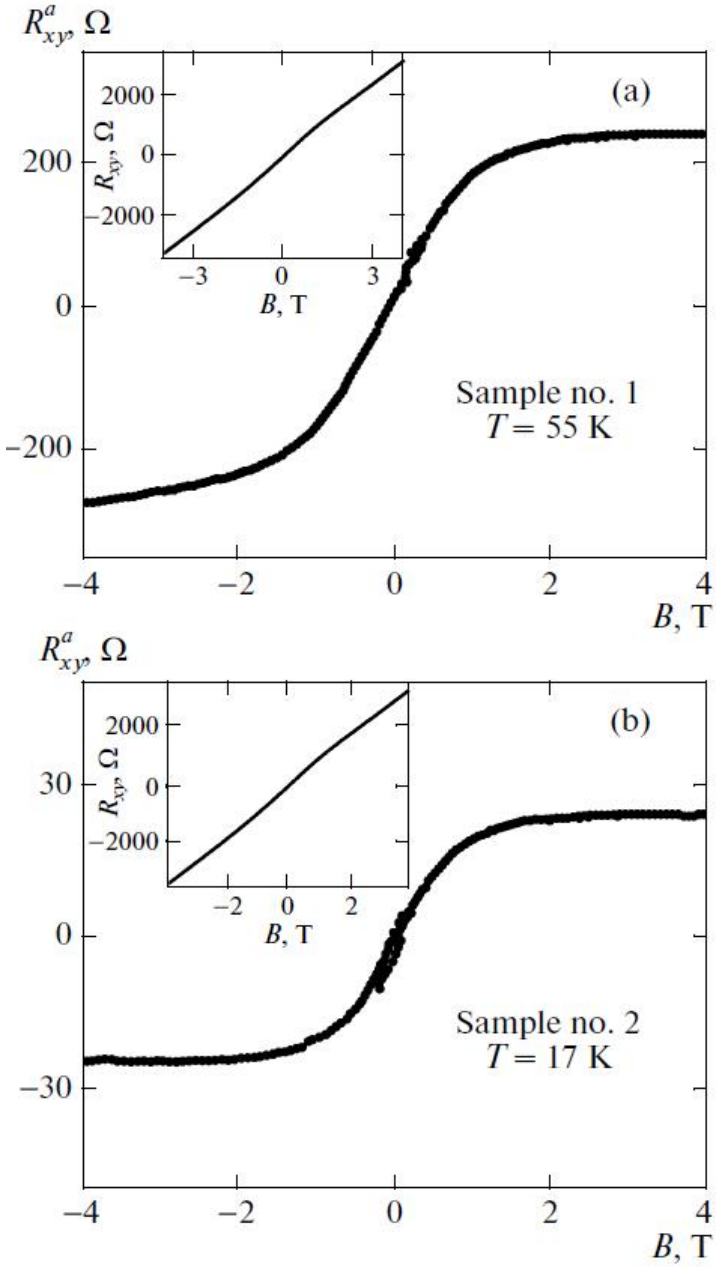

Figure 3.4. The anomalous Hall effect for the samples GaAs/Mn/GaAs/$In_xGa_{1-x}As$/GaAs structure [6]. Its appearance supposes the interaction of holes with manganese atoms and the establishment of ferromagnetic ordering [6]. Insets show the magnetic field dependences of the total Hall resistance [6].

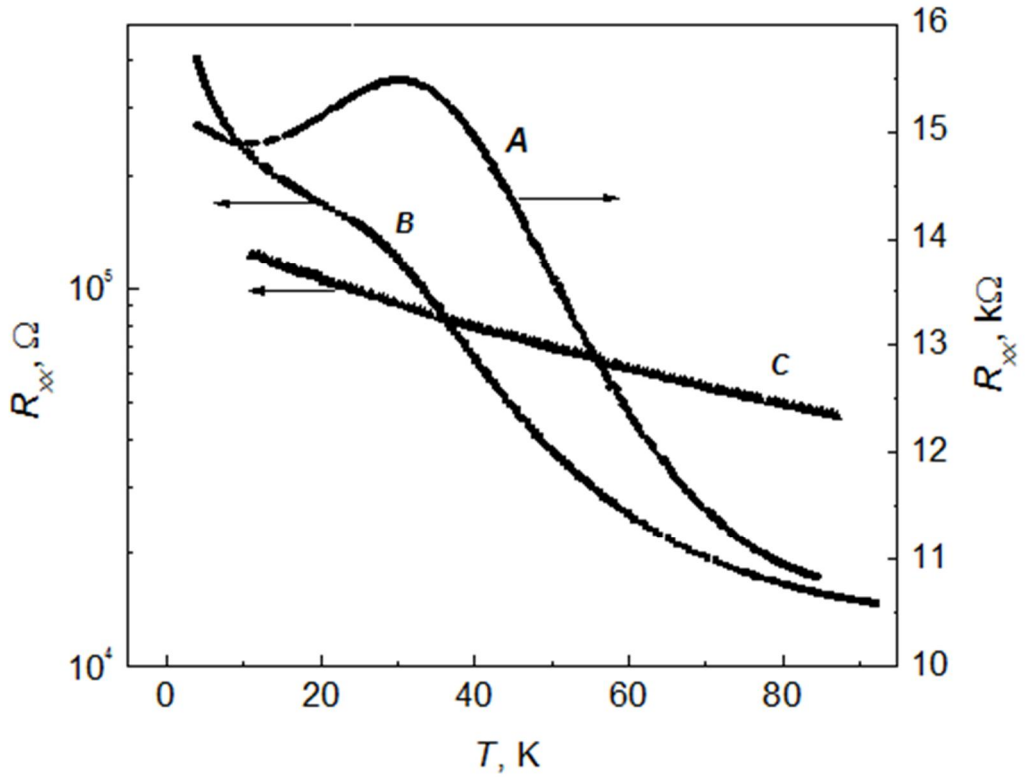

Figure3.5. Temperature dependences of the resistance R_{xx} for different GaAs/Mn/GaAs/$In_xGa_{1-x}As$/GaAs samples [5]. The maximum for curve A and the point of inflection for curve B indicate the Curie temperatures T_c [5].

In [5] the data of magnetization dependencies vs. magnetic field for samples A and B were also studied and are illustrated in Figs. 3.6a and b, correspondingly. They describe the case when the magnetic field is parallel to the plane of the samples. During the calculations the parasitic signals from the sample holder and the substrate were taken into account and subtracted from the measuring magnitude [5]. It caused a small distinction of the left parts of Fig. 3.6 and 3.7 from its rights parts, respectively. The main feature of these graphs is the presence of the shifted hysteresis loop. In general, the hysteresis loop is common for materials with ferromagnetic ordering and usually observed in strong magnetic fields [5]. However, as it is demonstrated in Figs. 3.6 and 3.7, magnetization was measured in weak magnetic fields and the results of such measurements correspond mainly to paramagnetic materials [5]. Special attention also should be paid to the shift of the hysteresis loop from $B_h \sim 0$ to higher

fields. For instance, for sample B B_h is approximately equal to 1 (see Fig. 3.6*b*). The exceeding of B_h for sample A in comparison with sample B is connected to the fact that sample B contains more manganese [5]. Thus, to induce the ferromagnetic ordering in the sample A the higher field is necessary [5].

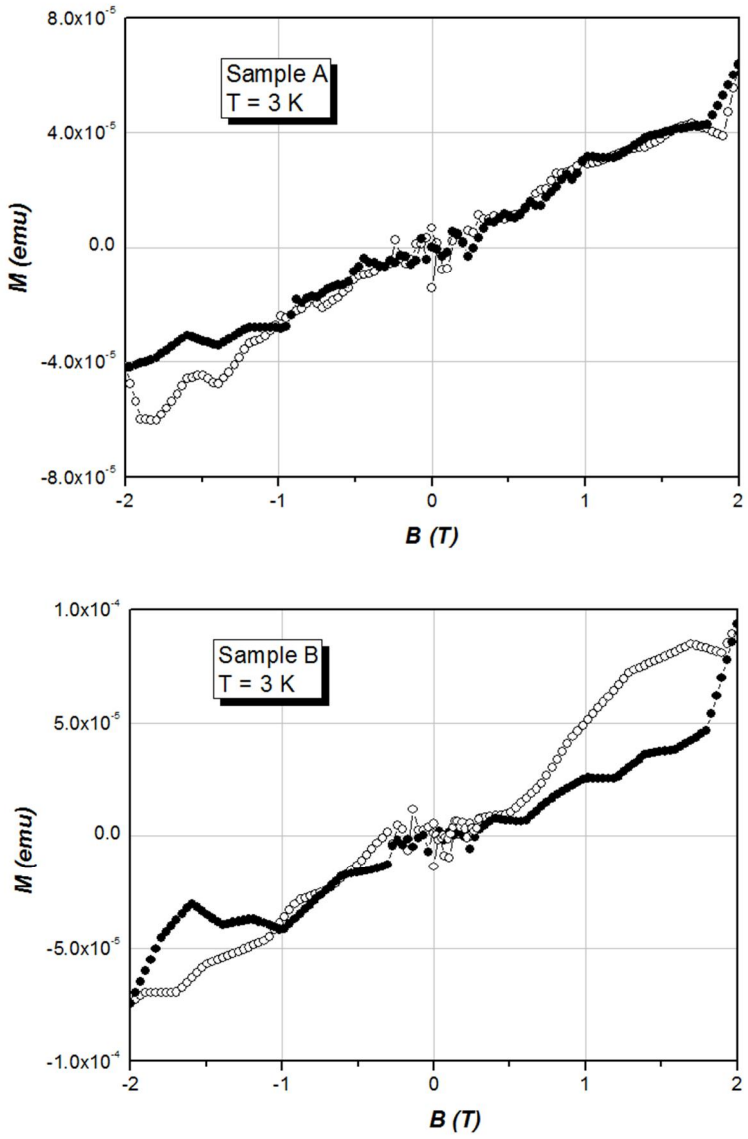

Figure 3.6. Magnetic field dependences of the magnetization for sample A (*a*) and B (*b*) GaAs/Mn/GaAs/$In_xGa_{1-x}As$/GaAs [5]. Magnetic field is parallel to the plane of the samples. The observation of hysteresis loop in such fields implies paramagnetic properties of the material [5]. Due to higher concentration of manganese in sample B the hysteresis loop is shifted to higher fields in comparison with sample A [5].

Thereby, there is a range of experimental phenomena observed in GaAs/Mn/GaAs/$In_xGa_{1-x}As$/GaAs, which are in good agreement with theoretical calculations of two-dimensional theory of energy spectrum of the carriers: the occurrence of Shubnikov–de Haas oscillations in the presence of magnetic field perpendicularly oriented to the plane of the sample, the calculation of the anomalous component of the Hall effect in weak magnetic field, ferromagnetic ordering of Mn atoms in δ-layer. It means that the earlier investigation of such structures show the perspective of studies of this material with the purpose of development of two-dimensional theory for diluted magnetic semiconductors.

4 EXPERIMENTAL SETUP

4.1. Fixing of the samples

The first step of the preparation of investigated samples for experiments is obtaining such overall dimensions of the samples, which satisfy the sizes of specially designed sample holder. For that reason an investigated material is cut with a diamond disk into pieces of rectangular shape. After that they are polished and put into a jar with kerosene for purification of their surfaces from chemical and mechanical inclusions.

The next step is to make contacts. Six indium contacts were smeared on each sample with configuration shown in Fig. 4.1.

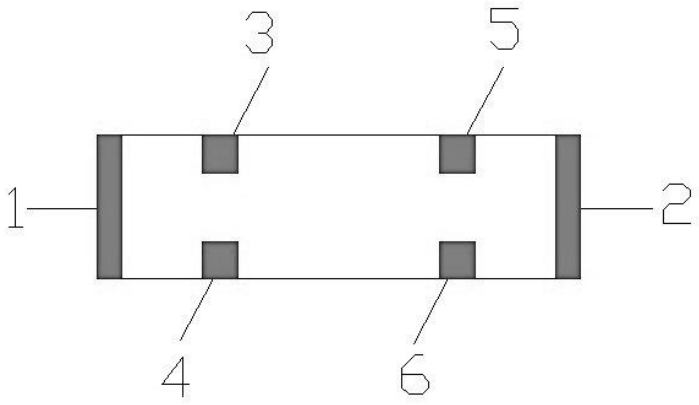

Figure 4.1. The scheme of disposition of the contacts on the sample.

For further processing the results, the distances between the contacts on the samples were measured by a trammel and are presented in Table 4.1. Thickness of each layer in the sample was measured by the small angle X-ray diffraction. The photo of the sample under a microscope is presented in Fig. 4.2.

Table 4.1. Distances between the contacts on the sample.

L_{12}, cm	0.480
L_{35}, cm	0.195
L_{46}, cm	0.185
L_{36}, cm	0.125
L_{45}, cm	0.125
W_{34}, cm	0.150
W_{56}, cm	0.155
W_{36}, cm	0.100
W_{45}, cm	0.100

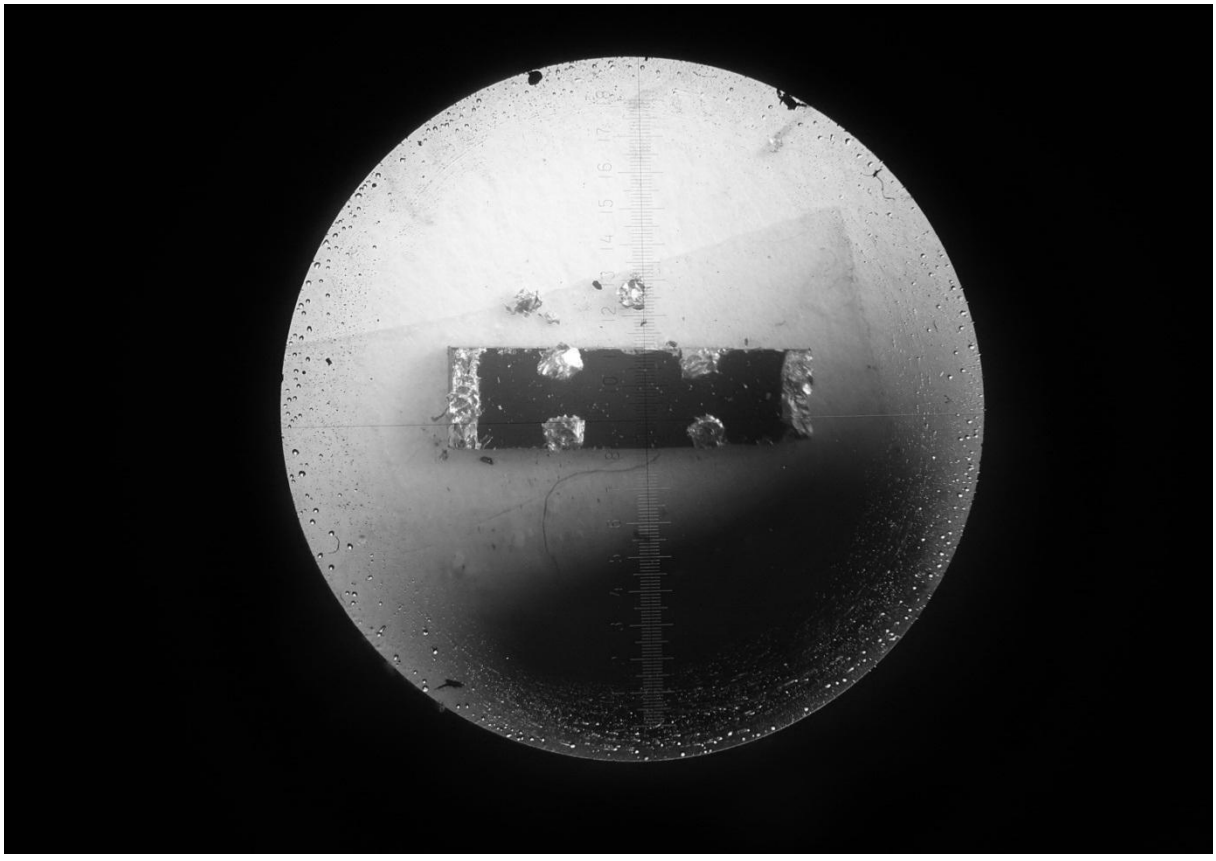

Figure 4.2. Photo of the sample with contacts.

The contacts for the sample are connected to bornier on the sample holder by copper wires with diameter 0.3 mm in double silk insulation. The wires were fastened to the contacts on the sample by smearing and pressing and to the bornier by soldering. An alloy of tin and lead in a ratio 60/50 respectively was used as a solder alloy. In order to reduce self-induction all the wires were twisted together. After that the sample was put into the sample holder (see Fig. 4.3) in which were installed such elements as coil for magnetic field measurements and compensation coil, a sample heater, Au-Fe and Cu-Fe thermocouples, a pressure sensor and a level gauge of liquid helium. The sample holder in its turn was fixed into the cryostat and its end with the sample was inserted inside pulsed solenoid.

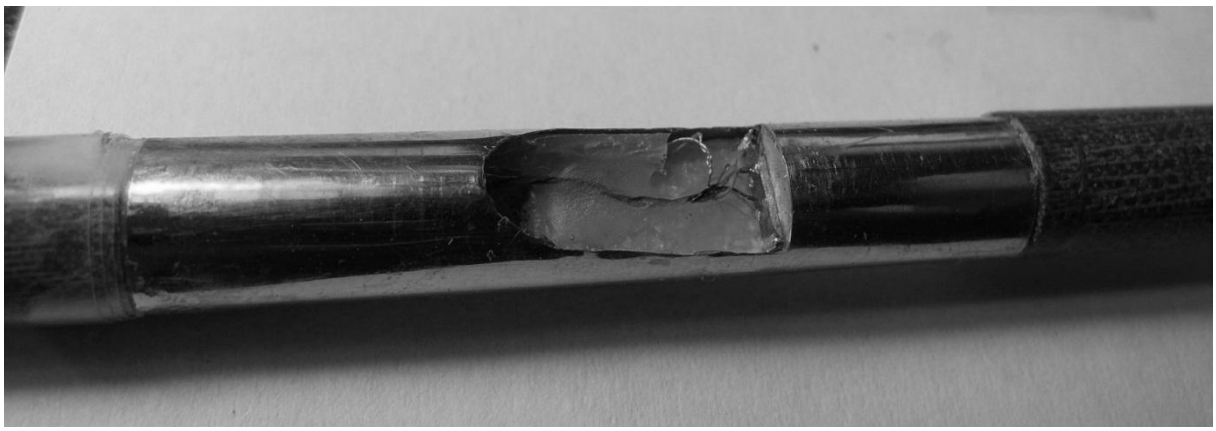

Figure 4.3. Sample inside the sample holder.

In processing the results an assumption about the isothermal continuous for the sample was made. This assumption is due to the fact that the time of a single pulse (11 ms) is much smaller than the time needed for heat transfer through the sample.

4.2. Description of experimental setup

4.2.1. Principal of operation and main parameters

This experimental work was done with a setup designed in a purpose of investigation of galvanometric properties of solids in pulsed magnetic fields. The setup, called Pulsed Magnetic Field System (PMFS), operates in a range of temperatures 1.6 – 350 K and

magnetic fields up to 45 T. The photos of the PMFS and its block diagram are presented in Fig. 4.4 and 4.5, respectively.

Figure 4.4. Photos of the Pulsed Magnetic Field System. Place of operator (upper photo) and the PMFS itself (lower photo).

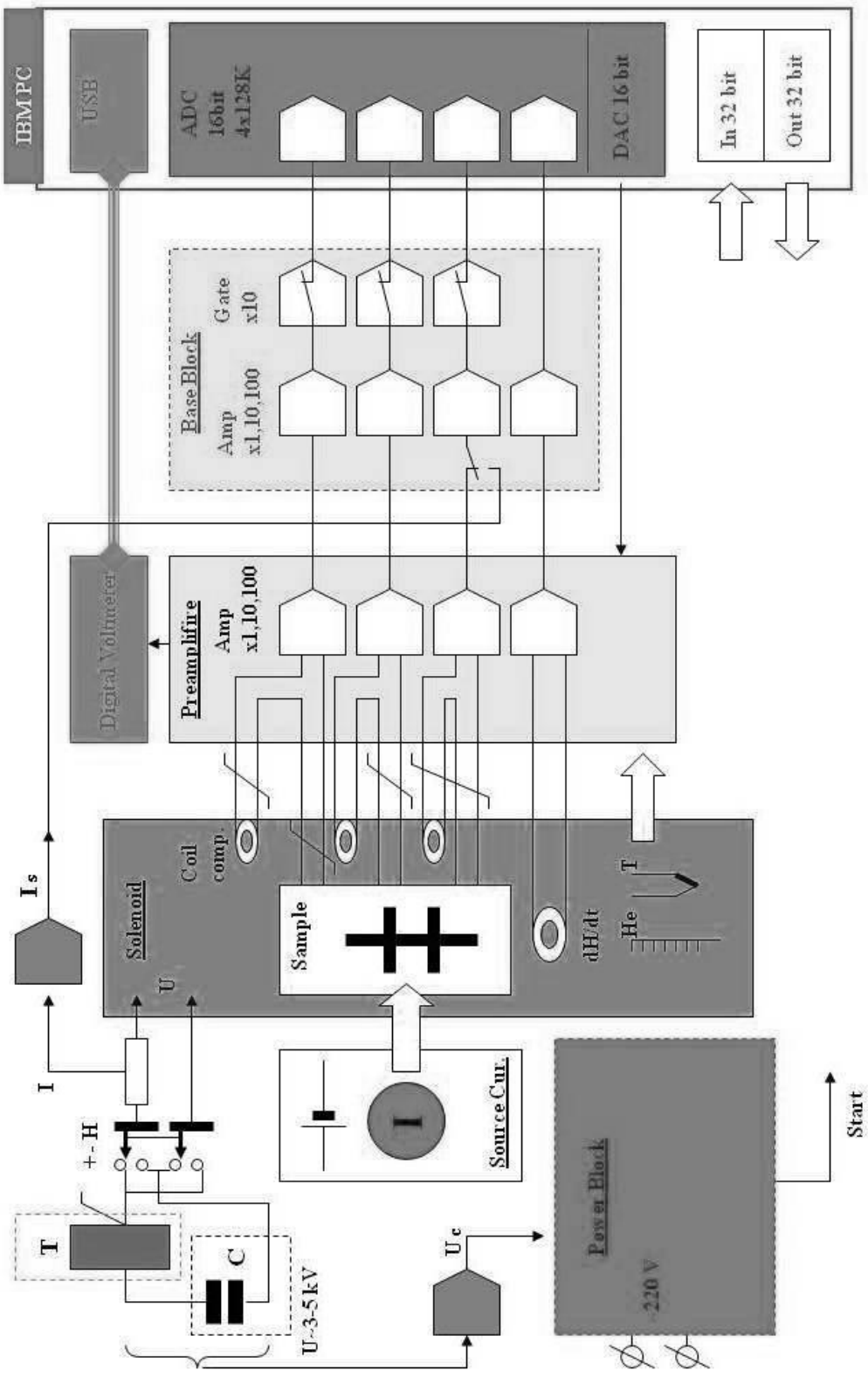

Figure 4.5. The block diagram of The PMFS.

The main principle of operation of the PMFS is as follows. The discharging of the bank of capacitors through the solenoid generates a pulsed magnetic field. The charging of the capacitors (U_c) is controlled by Power Block and two voltmeters. The conversion of the energy stored in the capacitors into the energy of magnetic field pulses created by the solenoid is managed by an electric circuit included two blocks of thyristors. The polarity of magnetic field can be changed by means of the knife switch. Experiments can be carried out at low temperatures, therefore, the setup includes a cryostat. Sample holder is put into the cryostat, which has a finger where the sample has to be located. This finger is set inside the solenoid. The pulsed electric current source is responsible for supplying the sample by current. Measured signals from the contacts connected to the sample are amplified in the Preamplification Block and the Base Block and after that are processed by PC. Analog-to-digital (ADC) and digital-to-analog (DAC) converters are used for transformation of the type of the signals.

The main parameters of the PMFS in our experiments with the investigated material are presented in Table 2.2.

Table 2.2. The main parameters of the experimental setup.

Amplitude of the magnetic field, up to	45T
Maximum current of solenoid, up to	20 kA
Capacitor bank 10 mF x 5 kV	125 kJ
4 digital measurement channels	16 bit, 1μs, 4*256 Kbyte
Duration of the magnetic field pulse	~11 ms
Sensitivity limited noise	~5 μV
Temperature range of operation	2 K – 350 K
Electric current of the sample	1 μA - 0.2 A
Range of the measured resistances	0.01 Ohm – 100 kOhm
Maximum voltage	5000 V

4.2.2. Hardware

The hardware of the PMFS can be divided into three main functional blocks: block of generation of pulsed magnetic field; cryogenic block and block of amplification system and additional equipment.

4.2.2.1. Block of generation of pulsed magnetic field

In the PMFS the generation of pulsed magnetic field is realized by means of discharging of energy stored in the bank of capacitors (see Fig 4.6) through the solenoid. The volume of magnetic field is about several cubic centimetres and the duration of pulses is several milliseconds.

Figure 4.6. The bank of capacitors.

Solenoid is one of the most important parts of the block of generating of pulsed magnetic field. In this setup it is a multiturn coil, which is made without magnetic materials in its construction to reduce the noise level and, therefore, to increase accuracy of measurements. The solenoid is wounded with flat insulated copper wire with usage of epoxy resin Stycast 2850FT. The schematic draft of the solenoid is shown in Fig. 4.7.

Second important part of this block, the pulsed electric current source, was specially designed for this PMFS. The main features of this device are its high impedance output and low noise characteristics. It operates by using the energy stored in the internal accumulators. The image of the front panel of the pulsed electric current source is presented in Fig. 4.8.

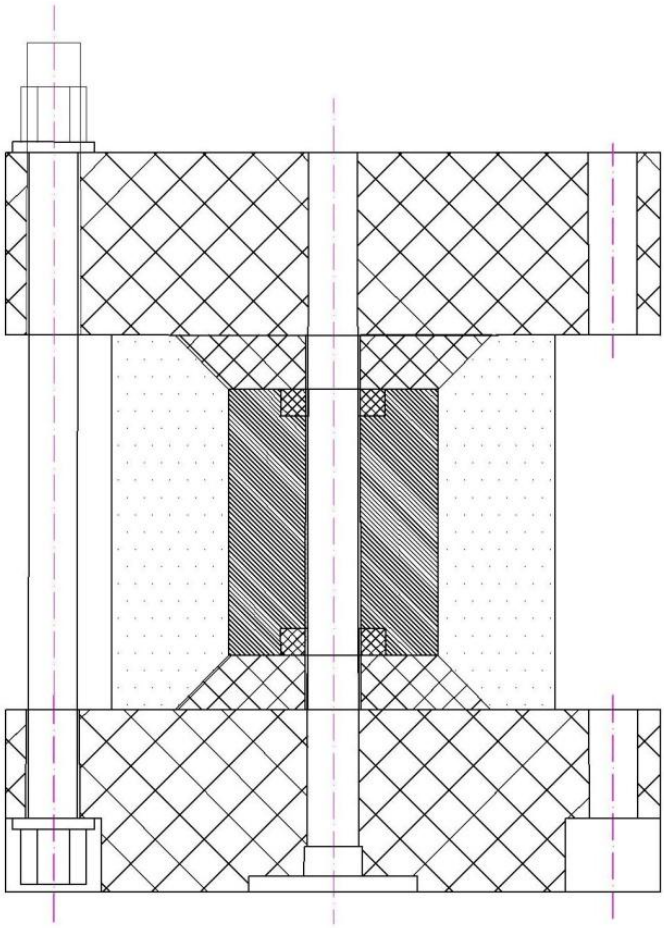

Figure 4.7. The schematic draft of the solenoid.

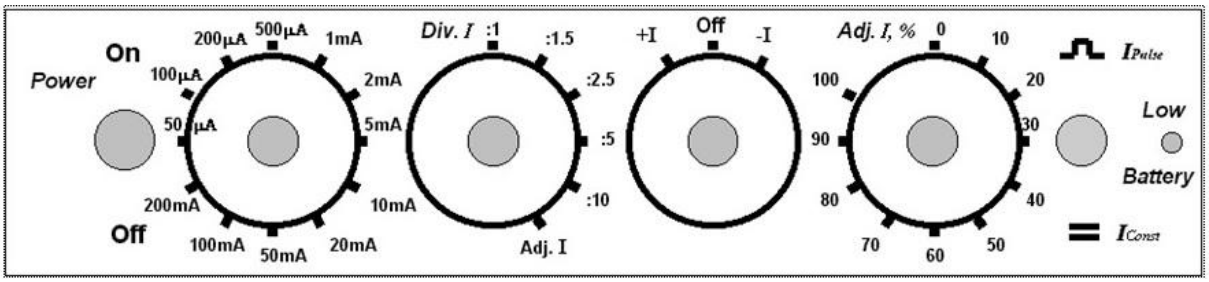

Figure 4.8. The front panel of the pulsed electric current source.

To generate magnetic field pulses the solenoid uses energy accumulated in the capacitors. They consist of separate devices with the capacity of 2750mkF per unit. The charging of the capacitors to the required voltage is implemented by high voltage rack located in the place of operator. The discharging circuit for the capacitors includes two separated blocks of thyristors T630, which characteristics are provided in Table 2.3.

Table 2.3. The characteristics of the discharging circuit.

Maximum peak current, up to	20 kA
Range work electric voltage	25 V - 6 kV
Capacitors bank 5-10 mF * 5 kV	~100 - 125 kJ
Duration of the current discharging on the solenoid	~1 - 100 ms
Minimum load inductance	40 μH
Maximal speed rate voltage dU/dt	200 V/μs
Time between maximum pulsing	~30 minutes
Maximum voltage	5000 V

The Power Block is responsible for controlling the system of generation of magnetic pulses is. It is located in the place of operator of the setup.

4.2.2.2. Cryogenic block

To carry out experiments at low temperatures specific cryostat (see Fig. 4.9) was designed and constructed for the PMFS.

Figure 4.9. Cryostat of the PMFS.

The cryostat has three straight pipes for pouring of liquid nitrogen and lateral outlet for gaseous helium. Filling with liquid helium is accomplished with a pipe, which is introduced into the sample holder. The sample holder is inserted into the cryostat by means of upper vertical pipe and has an input for a syphone, which can be connected to a transport liquid helium Dewar. The cryostat consists of upper nitrogen and lower helium sections. These sections are isolated by vacuum from each other. The helium section is protected by a copper shield to prevent radiation losses. This section ends up with the inner finger. It is placed inside the solenoid and together with the solenoid it is in a barrel with liquid nitrogen for cooling. The inner finger is also vacuum isolated from the liquid nitrogen surrounding. The photo of the cryostat installed into the setup is presented in Fig. 4.10.

Figure 4.10. Cryostat installed into the PMFS.

The vacuum in the cryostat is created by mechanical pump Alcatel 2012A, photo of which is shown in Fig. 4.11. Further improvement of vacuum occurs when activated carbon placed inside vacuum space of the cryostat is cooled down through the thermal contact with the section of liquid helium.

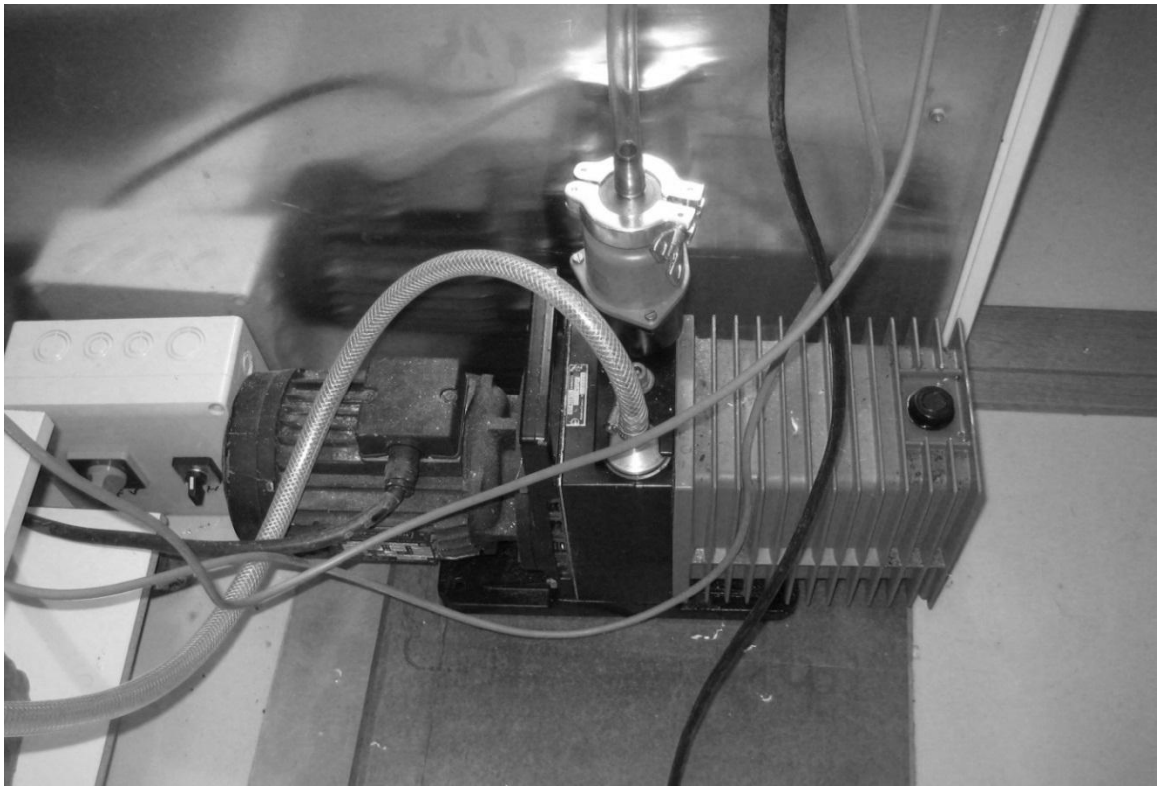

Figure 4.11. Photo of mechanical pump Alcatel 2012A.

Before carrying out the experiments the cryostat was modified. Its initial rubber gasket was replaced with aluminum gasket with indium insertion, the schematic draft of which is shown in Fig. 4.12. This change was due to the fact that the previous rubber gasket was exposed to strong low-temperature deformations.

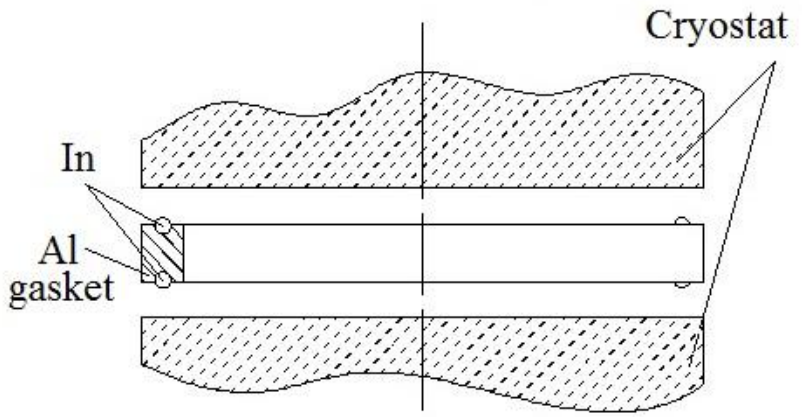

Figure 4.12. The schematic draft of aluminum gasket with indium insertion.

4.2.2.3. Block of amplification system and additional equipment

To increase the input signals the amplification system is designed and built in the PMFS. It consists of two blocks: the preamplification block and the base block. The latter also includes two section of amplifiers: the input section and the gate section. Manual and automatic changing of the voltage gains in amplifier circuits allow receiving of improved output signal, which is directed then to the analog-to-digital converter (ADC). The particularity of the amplification system of the setup is a possibility to change the amplifier voltage gain only during the activity of magnetic field. It provides an opportunity to allocate a signal dependent only on the magnetic field.

For reliable work of the setup and control of measuring values a range of additional equipment is used in the PMFS. The breakdown installation is performed as a separate mobile block including rectifiers, current limiting resistors, filters feeding and high voltage power transformers. For the purpose to monitor and regulate temperature of the sample, a thermocontroller LakeShore330 is in use. The multimeter Keithley 200 is used for measuring voltage values of such parameters as pressure created in the cryostat by the vacuum pump, helium level in the cryostat, temperature of the sample registered by thermocouples. Photos of thermocontroller and multimeter are presented in Fig. 4.13.

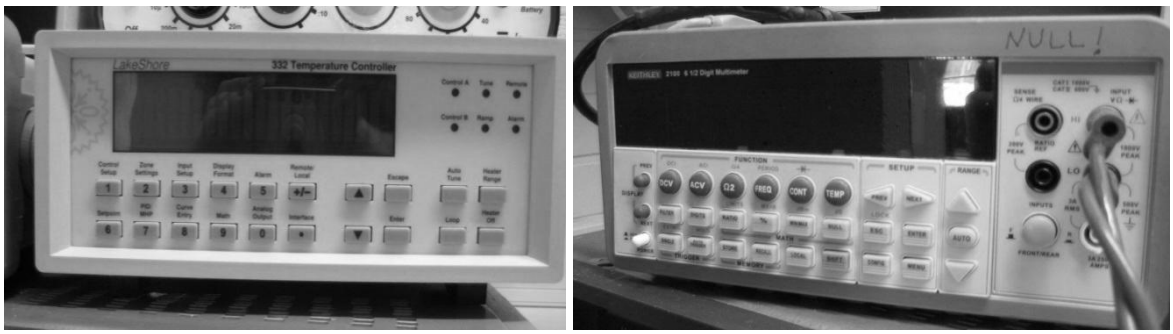

Figure 4.13. Thermocontroller LakeShore330 (left-hand side) and multimeter Keithley 200 (right-hand side).

4.2.3. Software

The PMFS has special software for processing of measurements. This software allows setting up initial experimental parameters (polarity and value of magnetic field and current through the sample, synchronization signals); distant controlling of functional blocks of the setup, for example, recharging of the capacitors; estimating of average lifetime and current technical condition of the solenoid; superposing of received signal for opposite polarities of magnetic field. Moreover, the compatibility with other data handling programs is also an important factor for further work with experimental results.

The software was designed using development environment LabVIEW. This development environment is widely used by engineers for graphical programming and hardware integration to design and deploy measurement and control systems. By means of LabVIEW, was created a range of virtual instruments, which help to reflect specifics of physical experiments done on this setup and regulate and control output data during the experiments.

For instance, there exist options to calibrate and control measuring and converting devices. An example of such approach is the module “GainsCompShow.vi”, which provides information about current condition of the amplification system. The image of the interface of this module is presented in Fig. 4.14.

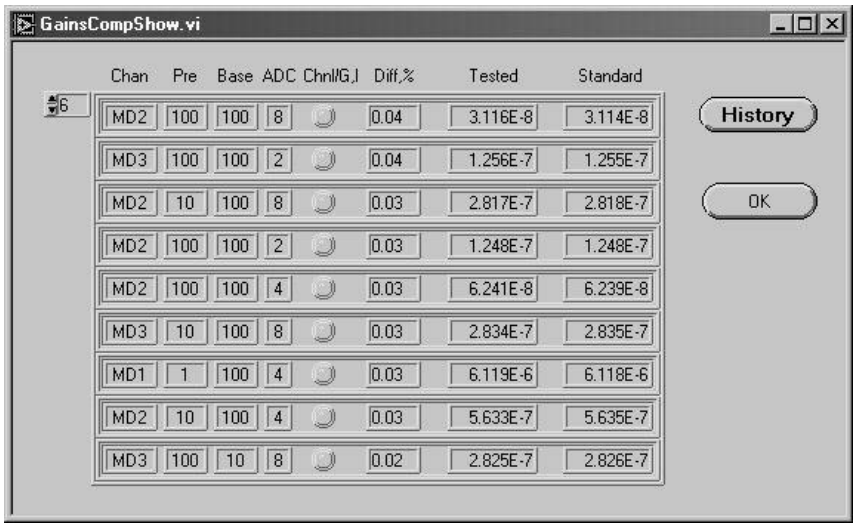

Figure 4.14. Module “GainsCompShow.vi”.

By means of the module “DetectPeack.vi” and original program “Oscillations detector”, it is possible to calculate amplitudes of oscillating components and positions of their extrema. These module and program were used in processing of Shubnikov-de Haas oscillations. The image of the interface of the program and the module are shown in Fig. 4.15 and 4.16, respectively.

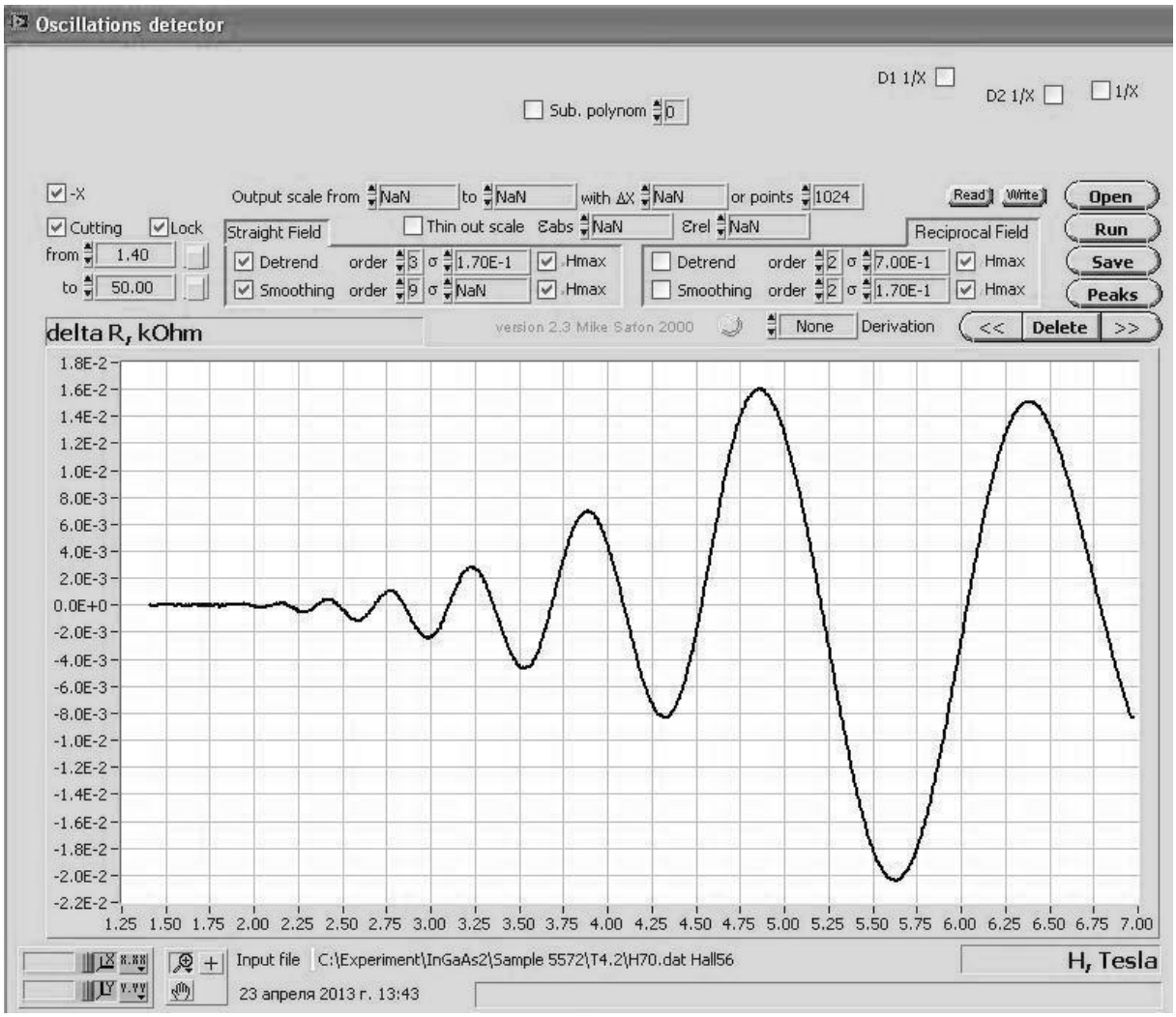

Figure 4.15. Interface of the program “Oscillations detector”.

As it is seen from Fig. 4.15, the basic functional buttons “Open”, “Run” and “Save” are located in the upper right part of the window of “Oscillations detector”. The central part of the window shows preliminary results of processing. By means of regulating output scale and functions of cutting and locking of definite parts of the dependence being processed it is

possible to obtain the results for given intervals of values. Moreover, “Oscillation detector” has an option to operate with several sets of data. The switching between the sets of data is done by the navigation buttons located in the upper right part of the window. In order to delete unnecessary sets of data the corresponding button, which is between the navigation buttons, is used.

Management of the processing of the results can be executed in two regimes: straight field and reciprocal field. For each of them there are functions of detrend and smoothing of obtained dependences. It is also possible to set definite degrees of polynomials for the mentioned functions. It should be noticed that “Oscillations detector” automatically choose a degree of polynomial for approximation of the data. However, the button “Sub. polynom”, which is located in the upper central part of the window, allows setting it manually. In the program there is also an option to plot the derivatives of different order.

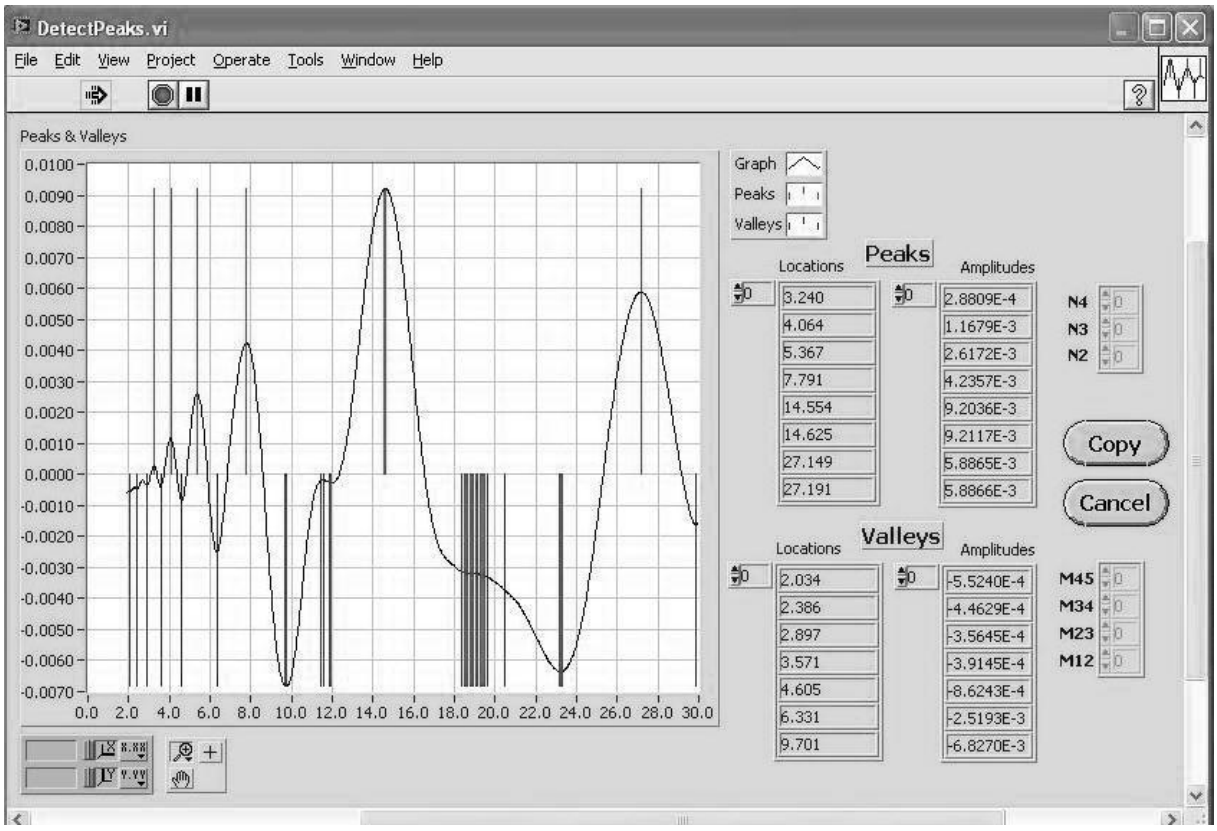

Figure 4.16. Module “DetectPeaks.vi”.

Switching to the module “DetectPeaks.vi” is performed by the button “Peaks”. This module provides information about the positions of peaks and values of the oscillations. Additionally, “DetectPeaks.vi” automatically calculates the amplitudes of the oscillations. For more comfortable work with the program the standard Windows panel was built is in the upper left part of the interface.

5 RESULTS AND DISCUSSION

During the experiments magnetic field dependences of the transverse magnetoresistivity and the Hall resistivity for GaAs/Mn/GaAs/$In_{0.15}Ga_{0.85}As$/GaAs structure were obtained in the temperature range 1.8 - 140 K. The anomalous Hall effect was detected and its component was subtracted from the total Hall effect. Shubnikov-de Haas oscillations were observed at 1.8 and 4.2 K. The calculation of the main characteristics of Shubnikov-de Haas oscillations were carried out.

5.1. Transverse magnetoresistance in temperature interval 33 - 140 K

Character of the transverse magnetoresistance was studied for temperatures 33, 50, 100, 120 and 140 K. For that reason the resistance of the sample was measured in the absence of magnetic field and in the presence of magnetic field up to 2.5 T aligned perpendicularly to the plane of the sample. Magnetic field dependence of the ratio of these two parameters is presented in Fig. 5.1.

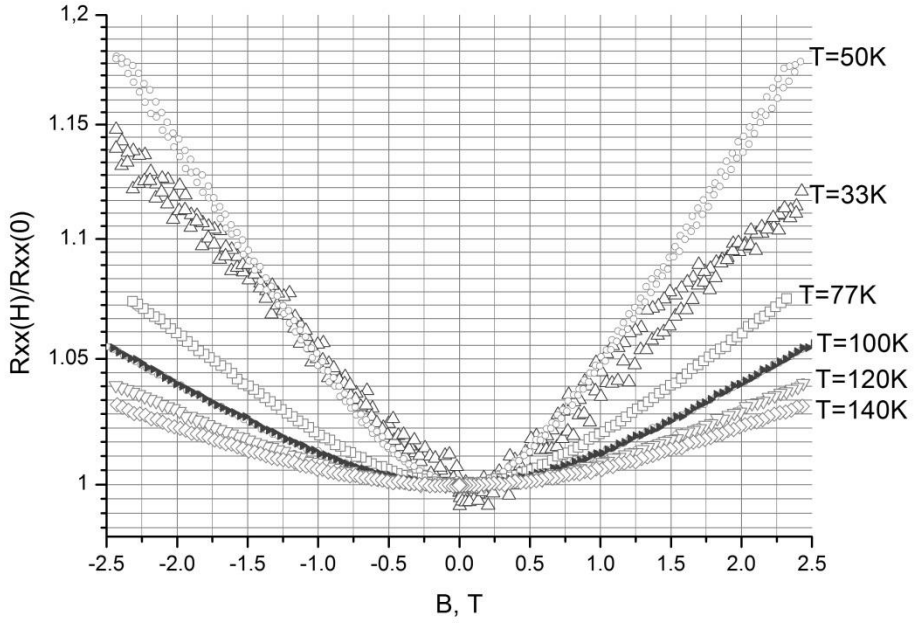

Figure 5.1. Magnetic field dependence of the ratio of the transverse magnetoresistance to the resistance in zero field. Structure GaAs/Mn/GaAs/$In_{0.15}Ga_{0.85}As$/GaAs demonstrates positive magnetoresistance.

As it can be seen from Fig. 5.1, the ratio of the transverse magnetoresistance to the resistance in zero field increases with growth of the intensity of magnetic field. It means that magnetoresistance for GaAs/Mn/GaAs/$In_{0.15}Ga_{0.85}As$/GaAs structure is positive in the temperature range of 33 - 140 K. It should be noticed that for temperature interval 50 - 140 K with decreasing of temperature the dependence becomes stronger. However, the curve for T = 33 K behaves differently: magnetic field dependence becomes weaker and near zero field an extremum is observed. Such behavior is in agreement with the results obtained in [6], where was defined that at approximately 30 K GaAs/Mn/GaAs/$In_xGa_{1-x}As$/GaAs structures undergoes ferromagnetic transition.

5.2. The anomalous Hall effect

During the investigation of the Hall effect for GaAs/Mn/GaAs/ $In_{0.15}Ga_{0.85}As$/GaAs structure presence of the anomalous Hall effect was detected. Magnetic field dependences of the total Hall resistance and its anomalous component at 140, 50 and 33 K are presented in Figs. 5.2, 5.3 and 5.4, respectively. In order to obtain magnetic field dependences of the anomalous Hall resistance the special technique was used. At first, the normal Hall coefficient was defined by means of measuring the Hall resistance in strong magnetic field when the normal Hall effect determines the total Hall effect and the contribution of the anomalous component can be neglected. Then, the corresponding normal Hall resistance was subtracted from the total Hall resistance and magnetic field dependence of the anomalous Hall resistance was obtained.

Figs. 5.2, 5.3 and 5.4 show that with decreasing of temperature the total Hall resistance becomes larger. Moreover, the contribution of the anomalous component is bigger at lower temperatures. The latter statement is deduced from analysis of the character of the curves, which describe magnetic field dependence of the total Hall resistance. When the contribution of the anomalous component is negligibly smaller with respect to the normal component the total Hall resistance is proportional to the intensity of magnetic field (see Eq. 2.21), thus, magnetic field dependence of the total Hall resistance has linear character. On the contrary, when the contribution of the anomalous component is essential, the dependence is nonlinear. At 140 K magnetic field dependence of the total Hall resistance represents a straight line (see

Fig. 5.2), at 50 K there is small deflection (see Fig. 5.3) and at 33 K the curve has a nonlinear character (see Fig. 5.4).

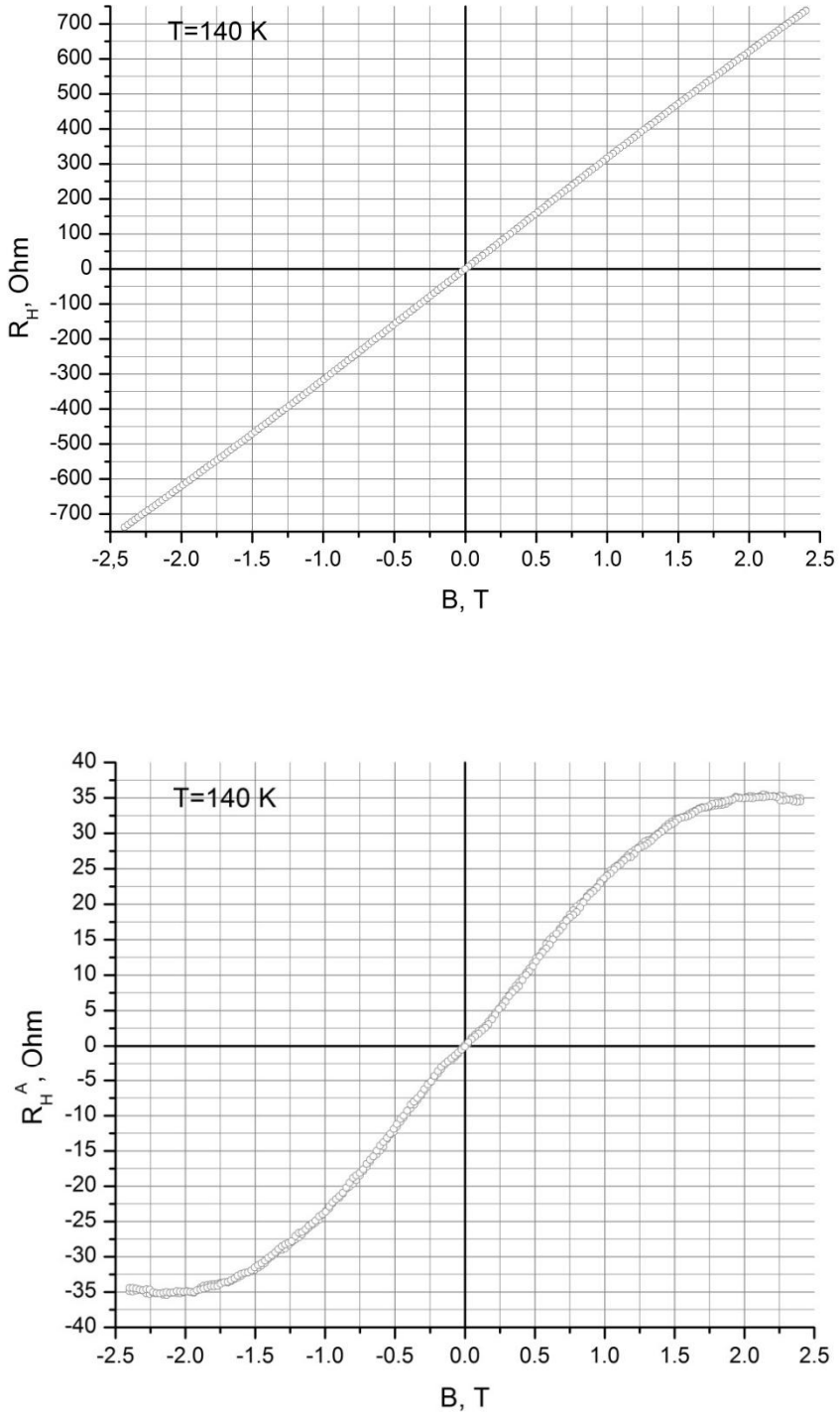

Figure 5.2. Magnetic field dependence of the total Hall resistance (upper figure) and the anomalous Hall component (lower figure) at 140 K.

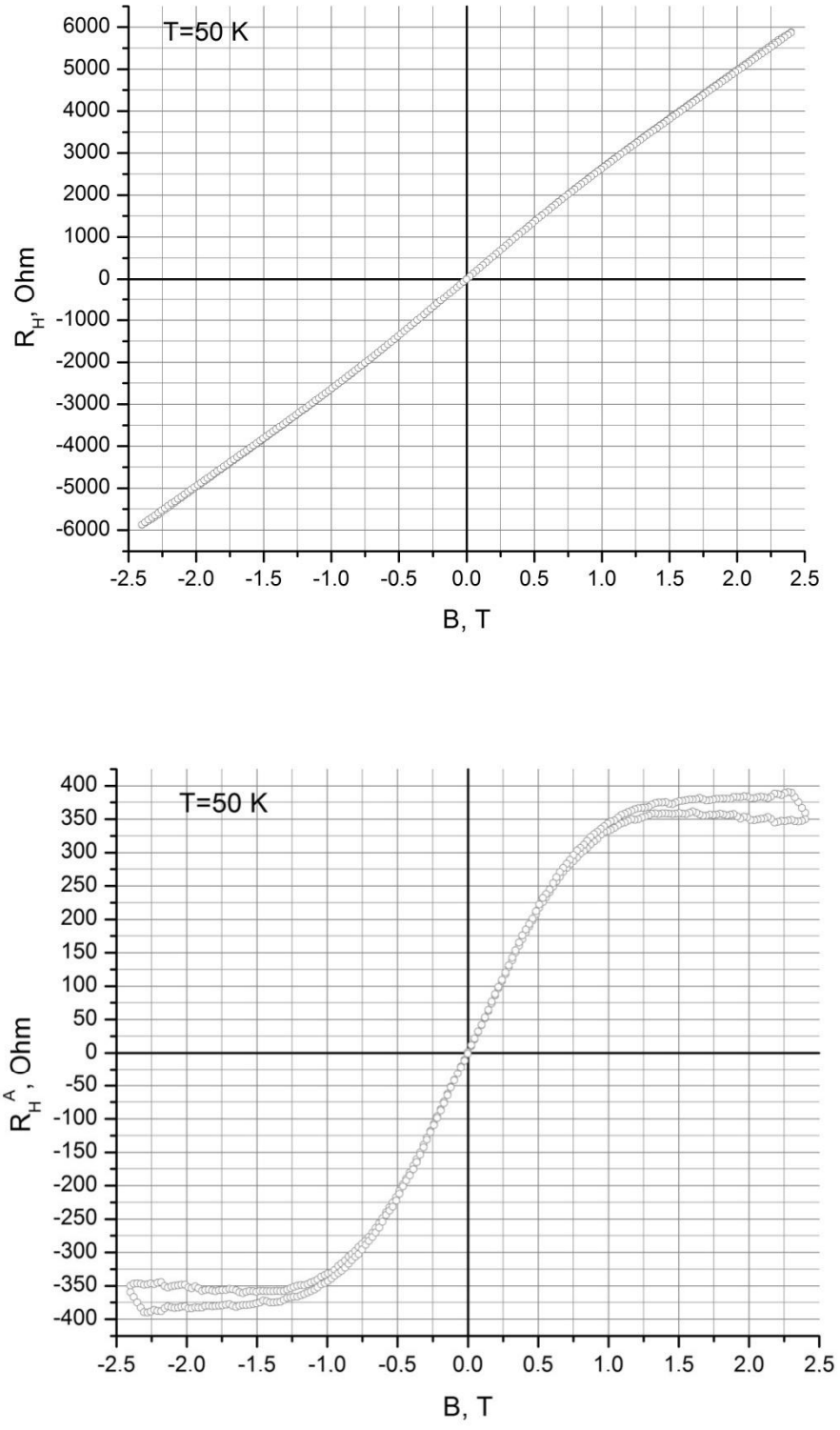

Figure 5.3. Magnetic field dependence of the total Hall resistance (upper figure) and the anomalous Hall component (lower figure) at 50 K.

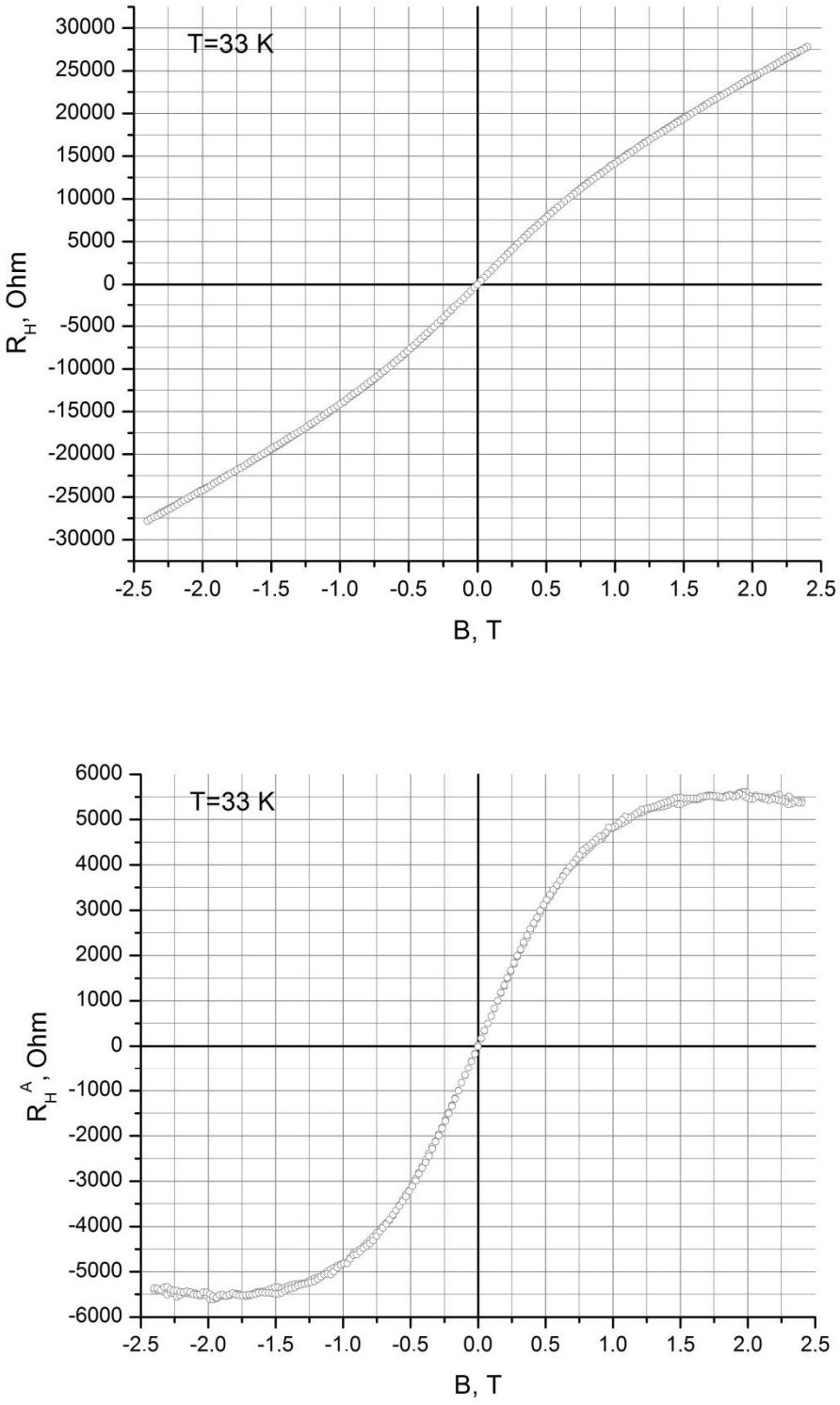

Figure 5.4. Magnetic field dependence of the total Hall resistance (upper figure) and the anomalous Hall component (lower figure) at 33 K.

5.3. Calculation of the energy band parameters from the Shubnikov-de Haas oscillations

The Shubnikov-de Haas oscillations were detected when measuring the transverse magnetoresistivity of GaAs/Mn/GaAs/$In_{0.15}Ga_{0.85}As$/GaAs sample at 1.8 and 4.2 K. Corresponding magnetic field dependences of the transverse magnetoresistivity are presented in Fig. 5.5.

Analyzing the dependences shown in Figs. 5.5 and using experimental data, it is possible to determine the period of Shubnikov-de Haas oscillations. For this purpose, the inverted values of the intensity of magnetic field which refer to the maxima of the transverse magnetoresistivity are plotted in correspondence with sequence of integers starting from 0. Then, these two arrays of the values are plotted. After the approximation of obtained results by straight line, the period of Shubnikov-de Haas oscillations can be calculated as its slope. The values of period of Shubnikov-de Haas oscillations obtained by using the experimental data measured at 1.8 K and 4.2 K are presented in Table 5.1.

Table 5.1. Period of Shubnikov-de Haas oscillations.

Temperature, T, K	Period of Shubnikov-de Haas oscillations, $P \cdot 10^{2}$, T^{-1}
1.8	5.26
4.2	5.12

Quantum numbers of Landau levels is determined by means of dividing initial array of integers by the calculated period. In Fig. 5.6 the inverted values of the intensity of magnetic field, which refer to the maxima of the transverse magnetoresistivity are put into correspondence with the numbers of Landau levels. It should be noticed that at 4.2 K the maxima for magnetic field $B > 10$ T are splitted (see Fig. 5.5). This was taken into account when plotting Fig. 5.6, which demonstrates two maxima with number of Landau level $N_m = 1$ and $N_m = 2$.

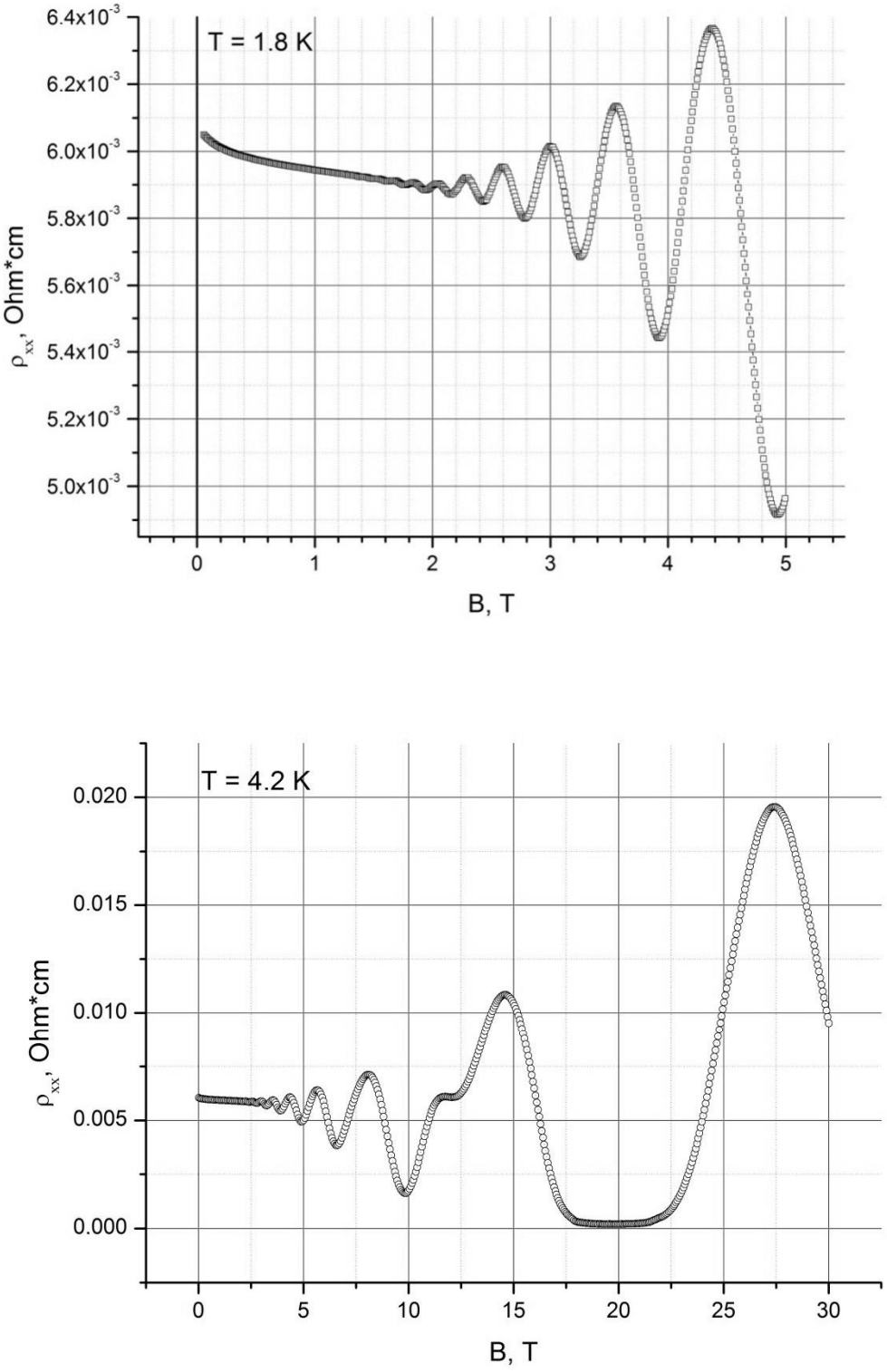

Figure 5.5. Magnetic field dependence of the transverse magnetoresistance at 1.8 K (upper figure) and at 4.2 K (lower figure).

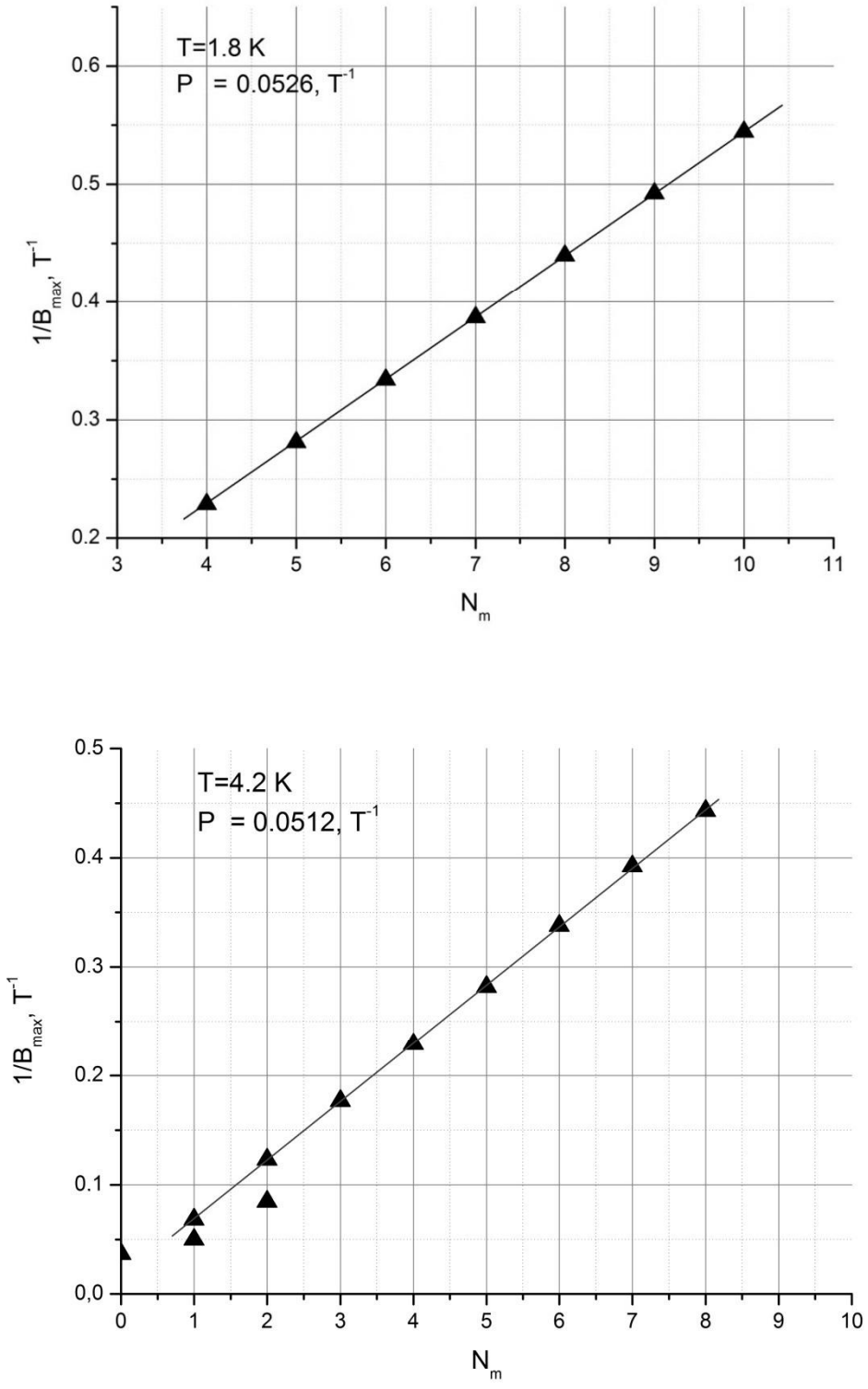

Figure 5.6. Determination of the period of Shubnikov-de Haas oscillations at 1.8 K (upper figure) and at 4.2 K (lower figure).

It is possible to define concentration of holes through the period of Shubnikov-de Haas oscillations. According to [30], the concentration of charge carriers p_{SdH} can be determined from the expression

$$P = \frac{2e}{ch(p_{\mathrm{SdH}})} = \frac{4.831 \cdot 10^{10}(T^{-1} \cdot cm^{-2})}{p_{\mathrm{SdH}}(cm^{-2})}. \quad (5.1)$$

On the other hand, the concentration of charge carriers can be found using the Hall constant R_H, which is determined as

$$R_{\mathrm{H}} = \frac{\rho_{\mathrm{xy}}}{B}, \quad (5.2)$$

where ρ_{xy} is the Hall resistivity and B is corresponding value of the induction of magnetic field [30]. In Fig. 5.7 magnetic field dependences of the Hall constant are presented at 1.8 K and 4.2 K.

Then before the beginning of oscillations (for $B \approx 1$ T) the Hall carrier concentration is calculated by the following formula

$$p_{\mathrm{Hall}} = \frac{1}{eR_{\mathrm{H}}}, \quad (5.3)$$

where R_{Hall} has dimension of cm^2/C [30]. Calculated values of the concentration of holes through the period of Shubnikov-de Haas oscillations and through the Hall carrier concentration, as well, as their ratio are presented in Table 5.2.

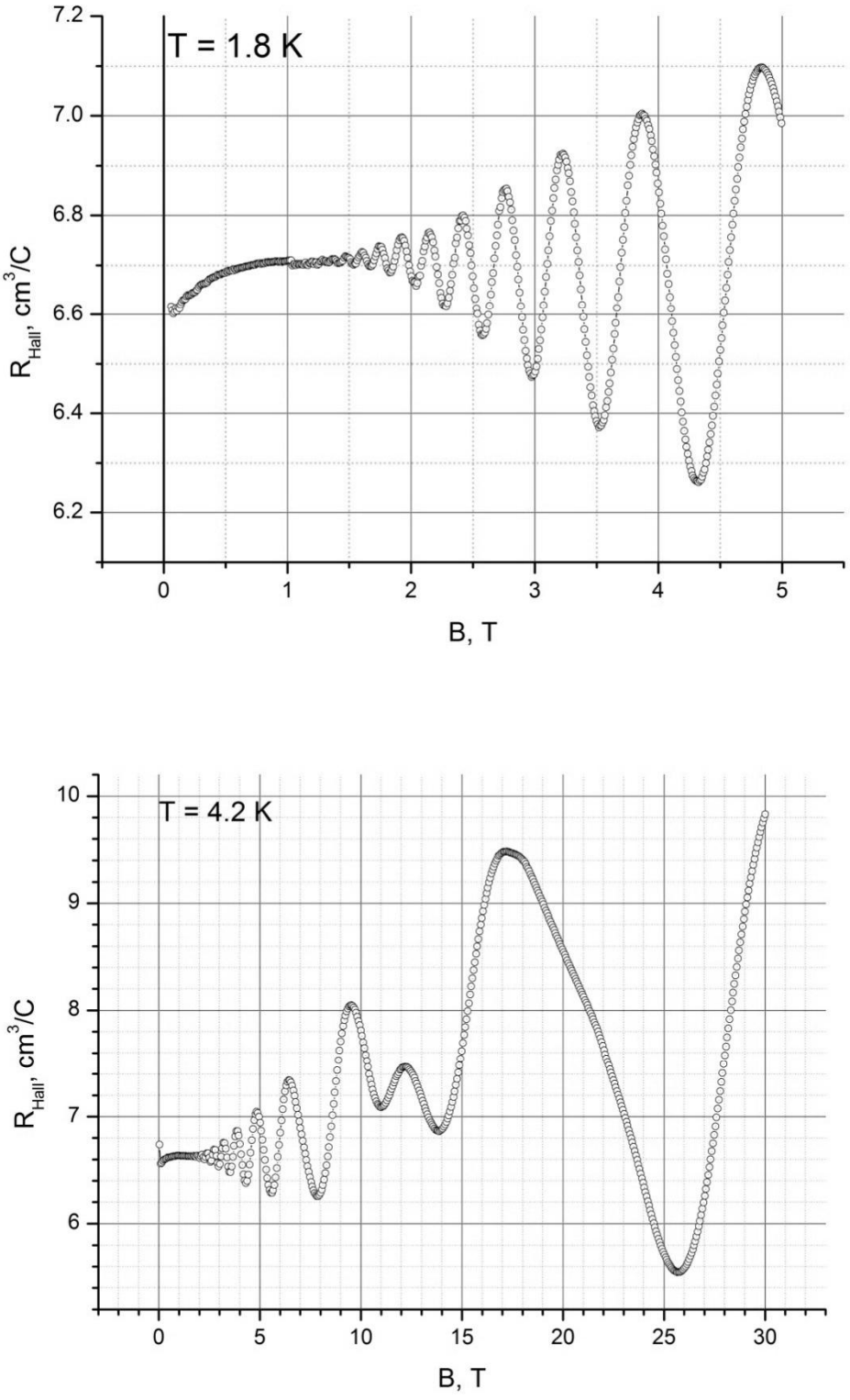

Figure 5.7. Magnetic field dependences of the Hall constant at 1.8 K (upper figure) and at 4.2 K (lower figure).

Table 5.2. Concentration of charge carriers (holes).

Temperature, T, K	Shubnikov-de Haas carrier concentration, $p_{SdH} \cdot 10^{-11}$, cm^{-2}	Hall carrier concentration, $p_{Hall} \cdot 10^{-11}$, cm^{-2}	$p_{SdH}/\ p_{Hall}$
1.8	9.18	9.33	1.016
4.2	9.44	9.42	0.998

It is clearly seen from Table 5.2 that the calculated concentration are approximately equal to each other $p_{SdH} \approx p_{Hall}$. This means that there is only one valence band, where holes are located.

Using Eqs. 2.36, 2.37 and 2.38, it is possible to calculate the ratio of cyclotron mass to the mass of free electron. In order to find the amplitudes A_i of Shubnikov-de Haas oscillations the module "DetectPeaks.fi" and program "Oscillations Detector" of the software of the PMFS is used (see chapter 4.2.3). The calculation gives the value of ratio of cyclotron mass to electron mass as

$$\frac{m_c}{m} = 0.12 \pm 0.03. \tag{5.5}$$

Furthermore, the Dingle temperature can be defined by two approaches: using the calculation of Shubnikov-de Haas oscillations and using the Hall mobility.

According to [4], the Dingle temperature $T_{D_{ShH}}$ is connected to the amplitudes of Shubnikov-de Haas oscillations by the following expression

$$A_i \approx \frac{x_i \cdot \exp\left(-2\pi^2 k_B T_{D_{ShH}}/\hbar\omega_c\right)}{(B_i E_F)^{1/2} \cdot sh(x_i)}, \tag{5.6}$$

where x_i is calculated by means of Eqs. 2.37 and 2.38 and E_F is the Fermi energy, which is determined as

$$E_F = \frac{\pi \hbar p_{\mathrm{SdH}}}{m_c}. \tag{5.7}$$

Analyzing Eq.5.6, it is possible to deduce that the Dingle temperature $T_{D_{ShH}}$ is defined by inclination of the dependence $ln\left(A_i(B_iE_F)^{1/2} \cdot sh(x_i)/x_i\right)$ on $1/B$. This dependence at 1.8 K and 4.2 K is presented in Fig. 5.8 and 5.9, respectively.

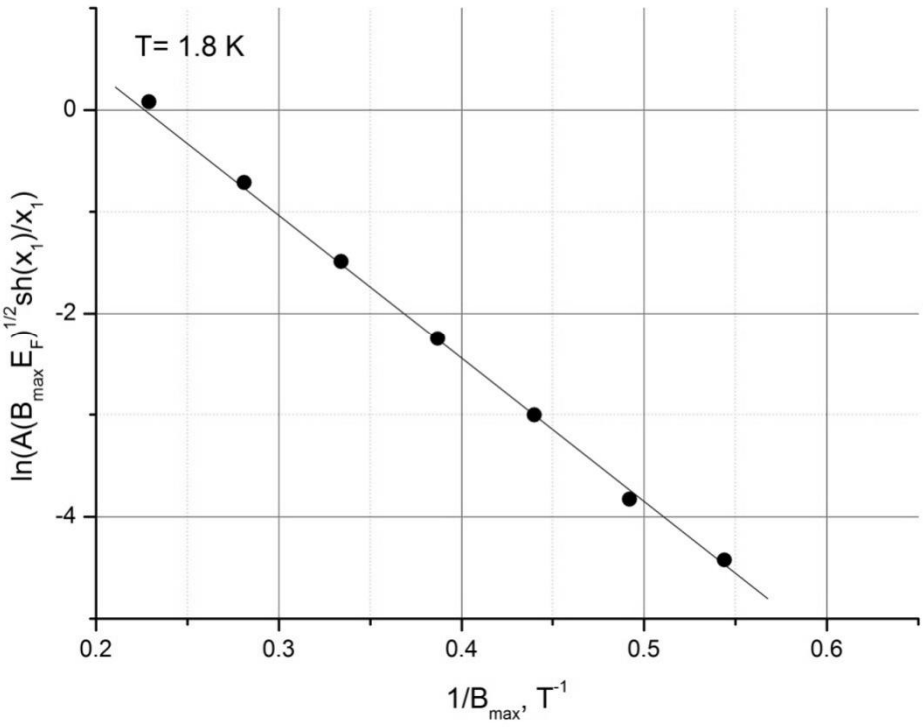

Figure 5.8. Determination of the Dingle temperature $T_{D_{ShH}}$ at 1.8 K.

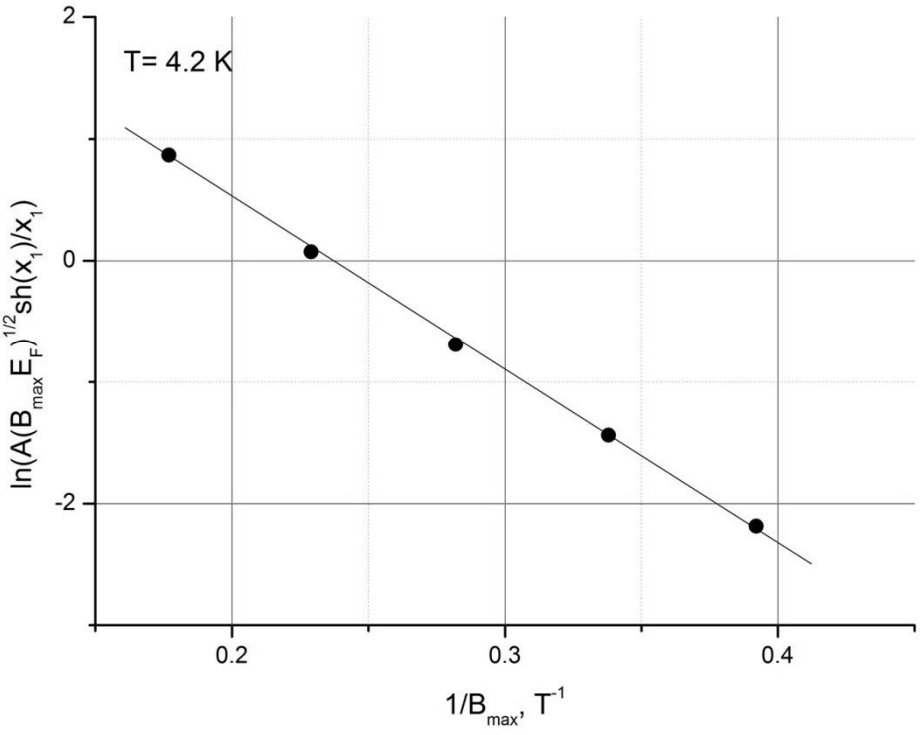

Figure 5.9. Determination of the Dingle temperature $T_{D_{ShH}}$ at 4.2 K.

Besides it, according to [4] and [30], the Dingle temperature is connected to the Hall mobility μ_{H}

$$T_{D_{Hall}} = \frac{\hbar e}{\pi k_B m_c \mu_{\mathrm{H}}}, \tag{5.8}$$

where μ_{H} can be defined by the following expression

$$\mu_{\mathrm{H}} = (R_{\mathrm{H}})^{\frac{3}{2}} \cdot \frac{1}{\rho_0}. \tag{5.9}$$

In Eq. 5.9 R_{H} is the Hall constant before the beginning of oscillations ($B \approx 1$ T) and $\rho_0 = R_{\mathrm{H}}(0)$.

In Table 5.3 are presented the values of the Dingle temperature calculated using the Hall mobility and using the parameters of Shubnikov-de Haas oscillations, as well as the Fermi energy and the Hall mobility.

Table 5.3. Results of calculation of the Dingle temperatures.

Temperature, T, K	Hall mobility, μ_H, cm^{-2}/Vs	Fermi energy, E_F, meV	Dingle temperature, $T_{D_{Hall}}$, K	Dingle temperature, $T_{D_{ShH}}$, K
1.8	2.62	23.8	1.4	14.3
4.2	2.54	24.5	1.4	14.2

From the comparison of the corresponding values of $T_{D_{Hall}}$ and $T_{D_{ShH}}$ in Table 5.3 it is possible to conclude that in our case the broadening of Landau levels is defined mainly by the scattering of charge carriers due to the defects of the crystal structure, but not due to temperature influence.

At 4.2 K the transverse magnetoresistivity (see Fig. 5.5) has splitting of the maxima with $N_m = 1$ and $N_m = 2$. As it was discussed before in chapter 2.3.3, g-factor must be calculated in order to take into consideration the splitting of maxima. According to [4], g-factor can be found as

$$g = \frac{2m_0\beta}{m_c}, \tag{5.10}$$

where β is the parameter, which is defined as

$$\beta = \frac{\Delta'}{P}, \tag{5.11}$$

where Δ' is determined as an average difference between the values of reciprocal magnetic induction for non-splitting and splitting maxima with the same number of Landau level N_m.

Calculated g-factor values and parameters Δ' and β are presented in Table 5.4.

Table 5.4. Parameters characterized splitting of the maxima.

Temperature, T, K	Δ', T^{-1}	β	g-factor
4.2	0.029	0.566	9.44

Thus, using the experimental data, the hole concentration was defined by two different approaches: using the period of Shubnikov-de Haas oscillations and using the Hall resisitivity. The comparison of these values of the hole concentration at corresponding temperatures showed that they were approximately equal to each other. Therefore, it can be concluded that all holes are located in one valence band.

For the investigated structure such important characteristic as cyclotron mass was calculated, which allowed determination of the Fermi energy and the Dingle temperature. It is also should be mentioned that the Dingle temperature was defined as well as the hole concentration, using two approaches. The results showed, that the Dingle temperature calculated by means of parameters of Shubnikov-de Haas oscillations had less magnitude than the Dingle temperature calculated using the Hall mobility. It means that in GaAs/Mn/GaAs/$In_{0.15}Ga_{0.85}As$/GaAs structure the broadening of Landau levels, which usually has thermal nature, is mainly determined by the scattering of charge carriers on the defects of crystal lattice.

Additionally, the calculation of g-factor, which characterizes spin splitting of the maxima of the transverse magnetoresistivity at 4.2 K, was performed.

6 CONCLUSIONS

The investigation of nanostructure GaAs/ Mn/ GaAs/ $In_{0.15}Ga_{0.85}As$/ GaAs conducted in this work allows making a number of conclusions about its galvanomagnetic properties and structural peculiarities.

By means of calculations conducted on the basis of experimental data the hole concentration in the quantum well of the investigated sample was estimated. At 1.8 K and 4.2 K it is approximately equal to $9.2 \cdot 10^{-11}$ cm^{-2} and $9.4 \cdot 10^{-11}$ cm^{-2}, respectively. It should be noticed that calculation of this value was carried out using two different approaches. The first one was performed through the parameters of Shubnikov-de Haas oscillations. The second one was implemented with use of the experimental data of magnetic field dependences of the Hall resistivity. It was shown that the ratio of the hole concentrations obtained by different approaches tends to be unit at corresponding temperatures. Such result confirms that for the investigated structure holes are located only in one valence band.

The observation of Shubnikov-de Haas oscillations gave possibility to estimate several galvanomagnetic and structural characteristics. The solution of the transcendental equation connecting the amplitudes of Shubnikov-de Haas oscillations and the position of its maxima at certain temperatures allowed determination of cyclotron mass. For our case it has value equal to $(0.12 \pm 0.03)m$, where m is a mass of free elecrtron. Determination of cyclotron mass made possible to define the Fermi energy, which is 23.8 meV and 24.5 meV at 1.8 K and 4.2 K, correspondingly, as well as the characteristic of imperfection of crystal structure, the Dingle temperature. The latter was calculated using two methods: through the parameters of Shubnikov-de Haas oscillations and through the value of Hall mobility. It should be mentioned that in order to perform calculation by the first method it was necessary to define the period of Shubnikov-de Haas oscillations. For that purpose was used special technique, which allowed determination of position of Landau levels. Meanwhile, in order to perform calculation by the second method the Hall mobility was initially calculated through the Hall constant. From the comparison of the Dingle temperatures obtained by application of two different approaches was concluded that the broadening of Landau levels in our case is mainly determined by the scattering of charge carriers on the defects of crystal structure.

The transverse magnetoresisitivity at 4.2 K showed the presence of several splitted maxima of Shubnikov-de Haas oscillations, which is explained by spin splitting of Landau levels. In order to characterize this phenomenon, *g*-factor was calculated. It has value approximately equal to 9.44.

Detection of the anomalous Hall effect confirmed presence of magnetic ordering in GaAs/Mn/GaAs/$In_{0.15}Ga_{0.85}As$/GaAs structure, which is typical for DMS. Additionally, positive character of the transverse magnetoresistance was defined for GaAs/ Mn/ GaAs/ $In_{0.15}Ga_{0.85}As$ / GaAs structure in the temperature range of 33 - 140 K.

Moreover, during the experiments technical skills of work with the PMFS were acquired. It includes control of its electrical parameters as well as maintenance of temperature conditions required in the experiments. Special attention was paid to study of main principals of operating with cryogenic liquids, nitrogen and helium. On the stage of preparation to the experiments two methods of making contacts to the sample were learnt: smearing and soldering. The software of the PMFS was also studied and certain additional modules of it were applied during the processing of Shubnikov-de Haas oscillations.

REFERENCES

[1] Zhang, Y. 2011. Electronic transport properties of semiconductor nanostructures. Doctoral dissertation. Stony Brook University.

[2] Hansen, L., Ferrand, D., Richter, G., Thierley, M., Hock, V., Schwarz, N., Reuscher, G., Schmidt, G., Waag, A. & Molenkamp L.W. 2001. Epitaxy and Magneto-transport properties of the diluted magnetic semiconductor p-$Be_{1-x}Mn_xTe$. *Applied Physics Letters*, vol. 79, No. 19, pp. 3125 - 3127.

[3] Jungwirth, T., Sinova, J., Masek, J., Kucera, J. & MacDonald, A.H. 2006. Theory of ferromagnetic (III,Mn)V semiconductors. *Reviews of Modern Physics*, vol. 78, No. 3, pp. 809 - 864.

[4] Oiwa, A., Endo, A., Katsumoto, S., Iye, Y., Ohno, H. & Munekata H. 1999. Magnetic and transport properties of the ferromagnetic semiconductor heterostructures (In,Mn)As/(Ga,Al)Sb. *Physical Review B*, vol. 59, No. 8, pp. 5826-5831.

[5] Aronzon, B.A., Lagutin, A.S., Rylkov1, V.V., Pankov, M.A., Lashkul, A.V. & Laiho, R. 2008. Disorder effects in GaAs/$In_xGa_{1-x}As$/GaAs quantum well delta doped with Mn. *Physics state solidi*, vol. 5, No. 3, pp. 814–818.

[6] Pankov, M.A., Aronzon, B.A., Rylkov, V.V., Davydov, A.B., Meilikhov, E.Z., Farzetdinova, R.M., Pashaev, E.M., Chuev, M.A., Subbotin, I.A., Likhachev, I.A., Zvonkov, B.N., Lashkul, A.V. & Laiho, R. 2009. Ferromagnetic transition in GaAs/Mn/GaAs/ $In_xGa_{1-x}As$/GaAs structures with a two-dimensional hole gas. *Journal of Experimental and Theoretical Physics*, vol. 109, No. 2, pp. 293-301.

[7] Bonch-Bryevich, V.L., Kalashnikov, S.G. 1977. Physics of semiconductors. Moscow: Nayka.

[8] Aronzon, B.A., Pankov, M.A., Rylkov, V.V., Meilikhov1, E.Z., Lagutin, A.S., Pashaev, E.M., Chuev, M.A., Kvardakov, V.V., Likhachev, I.A., Zvonkov, B.N., Lashkul, A.V., Lahderanta, E., Goiran, M. & Kervalishvili, P. 2010. Ferromagnetism in low dimensional structures of III-Mn-V semiconductors near metal-insulator transition [online document]. *Journal of Applied Physics*, vol. 136, No. 8. Available at http://dx.doi.org/10.1063/1.3267314

[9] Askerov, B.M. 1985. Electron Transport Phenomena in Semiconductors. Moscow: Nayka.

[10] Owen, M.H.S. 2010. Electrical gating effects on the magnetic properties of (Ga,Mn)As diluted magnetic semiconductors. Doctoral dissertation. University of Cambridge, Department of Physics.

[11] Aronzon, B.A., Rylkov, V.V., Nikolaev, S.N., Tugushev, V.V., Caprara, S., Podolskii, V.V., Lesnikov, V.P., Lashkul, A.V., Laiho, R., Gareev, R.R., Perov, N.S. & Semisalova, A.S. 2011. Room temperature ferromagnetism and anomalous Hall effect in $Si_{1-x}Mn_x$ ($x \approx 0.35$) alloys [online document]. *Physical Review B*, vol. 84, No. 7. Available at http://link.aps.org/doi/10.1103/PhysRevB.84.075209

[12] Rushforth, A. W., Vyborny, K., King, C. S., Edmonds, K. W., Campion, R. P., Foxon, C. T., Wunderlich, J., Irvine, A. C., Vasek, P., Novak, V., Olejnık, K., Sinova, J., Jungwirth, T. & Gallagher, B. L. 2007. Anisotropic Magnetoresistance Components in (Ga,Mn)As. *Physical Review Letters*, vol. 99, No. 14. Available at http://link.aps.org/doi/10.1103/PhysRevLett.99.147207

[13] Rushforth, A., Vyborny, K., King, C., Edmonds, K., Campion, R., Foxon, C., Wunderlich, J., Irvine, A., Novak, V., Olejnyk, K., Kovalev, A., Sinova, J., Jungwirth, T. &.Gallagher, B.L. 2009. The origin and control of the sources of AMR in (Ga,Mn)As devices *Journal of Magnetism and Magnetic Materials*, vol. 321, No. 8, 321, pp. 1001 – 1008.

[14] Otsu, H., Konigorski, D. & Abe, T. 2010. Influence of Hall effect on electrodynamic heat shield system for reentry vehicles. *AIAA Journal*, vol. 48, No. 10, pp. 2177-2186.

[15] Cidilkovsky, I.M. 1972. Electrons and holes in semiconductors.Moscow: Nayka.

[16] Nagaosa., N., Sinova., J., Onoda, S., MacDonald, A.H. & Ong, N.P. 2009. Anomalous Hall effect. *Reviews of Modern Physics*, vol. 82, No. 2, pp. 1539-1592.

[17] Karplus, R. & Luttinger, J.M. 1954. Hall Effect in Ferromagnetics. Physical Review, vol. 95, No. 5, pp. 1154-1160.

[18] Smith, J. 1955. The spontaneous Hall effect in ferromagnetics I. *Physica*, vol. 21, pp. 877-887.

[19] Smith, J. 1958. The spontaneous Hall effect in ferromagnetics II. *Physica*, vol. 24, pp. 39-51.

[20] Berger, L. 1970. Side-jump mechanism for the Hall effect of ferromagnets. *Physical Review B*, vol. 2, No. 11, pp. 4559-4565.

[21] Pu, Y., Chiba, D., Matsukura, F., Ohno, H. & Shi, J. 2008. Mott Relation for Anomalous Hall and Nernst Effects in $Ga_{1-x}Mn_xAs$ ferromagnetic semiconductors [online document]. *Physical Review Letters*, vol. 101, No. 11. Available at http://link.aps.org/doi/10.1103/PhysRevLett.101.117208

[22] Edmonds, K.W., Campion, R.P., Wang, K.Y., Neumann, A.C., Gallagher, B.L., Foxon, C.T. & Main, P.C. 2003. Magnetoresistance and Hall effect in the ferromagnetic semiconductor in $Ga_{1-x}Mn_xAs$. *Journal of Applied Physics*, vol. 93, No. 10, pp. 6787 – 6789.
[23] Chun, S.H., Kim, Y.S., Choic, H.K., Lee, W.O., Suhc, K.S., Oh, Y.S., Kim, K.H., Khim, Z.G. & Park, Y.D. 2007. Intrinsic anomalous Hall conductivity of GaMnAs solely governed by the carrier concentration. *Journal of Magnetism and Magnetic Materials*, vol. 310, No. 2, pp. 2064 – 2066.
[24] Ruzmetov, D., Scherschligt, J., Baxter D.V., Wojtowicz, T., Liu, X., Sasaki, Y., Furdyna, J.K., Yu, K.M. & Walukiewicz, W. 2004. High-temperature Hall effect in $Ga_{1-x}Mn_xAs$ [online document]. *Physical Review B*, vol. 69, No. 15. Available at http://link.aps.org/doi/10.1103/PhysRevB.69.155207
[25] Akiba, N., Chiba, D., Nakata, K., Matsukura, F., Ohno, Y. & Ohno, H. 2000. Spin-dependent scattering in semiconducting ferromagnetic (Ga,Mn)As trilayer structures. *Journal of Applied Physics*, vol. 87, No. 9, pp.6436-6438.
[26] Lashkul, A.V. 2007. Quantum transport phenomena and shallow impurity states in CdSb. Doctoral dissertation. Lappeeranta University of Technology, Department of Technomathematics and Technical Physics.
[27] Cidilkovsky, I.M. 1978. Energy band structure of semiconductors. Moscow: Nayka.
[28] Tarasenko, I.A. 2002. The effect of Zeeman splitting on Shubnikov–de Haas oscillations in two-dimensional systems. *Physics of the Solid State*, vol. 44, No. 9, pp. 1769–1773.
[29]. Freire, H. J. P & Egues, J.C. 2004. Shubnikov-de Haas Oscillations in Digital Magnetic Heterostructures. *Brazilian Journal of Physics*, vol. 34, No. 2b, pp. 614-616.
[30] Askerov, B.M. 1970. Kinetic Effects in Semiconductors. Moscow: Nayka.